Mixed proton-electron conducting oxides for high temperature hydrogen separation membrane

Wen Xing

Dissertation for the Degree of Philosophiae Doctor

Functional Energy Related Materials in Oslo

Centre for Materials Science and Nanotechnology

Department of Chemistry

Faculty of Mathematics and Natural Sciences

UNIVERSITY OF OSLO

2013

Series of dissertations submitted to the
Faculty of Mathematics and Natural Sciences, University of Oslo
No. 1382

ISSN 1501-7710

Cover: Inger Sandved Anfinsen.
Printed in Norway: AIT Oslo AS.

Produced in co-operation with Akademika Publishing.
The thesis is produced by Akademika Publishing merely in connection with the thesis defence. Kindly direct all inquiries regarding the thesis to the copyright holder or the unit which grants the doctorate.

Preface

This thesis represents parts of the work in fulfilment of the degree of Philosophiae Doctor (Ph.D) at the Department of Chemistry, Faculty of Mathematics and Natural Sciences, University of Oslo. This work has been carried out at Functional Energy related Materials in Oslo (FERMiO) during the period of April 2009 to April 2012 and been funded by the Research Council of Norway though the project of "BIGCO2".

First I would like to thank my supervisors: Associate Professor Reidar Haugrud, Professor Truls Norby and Doctor Zuoan Li for their endless enthusiasm and for sound scientific guidance in the past six years. Associate Professor Reidar Haugsrud has been my main supervisor and he was always ready to discuss scientific challenges and give the feedbacks in a short period. Professor Truls Norby led me to his group and material science field in the August of 2006 and has been particularly helpful with his optimism, encouragement and scientific knowledge. Doctor Zuoan Li has helped me both in English language and science with his patience and encouragment.

I would like to acknowledge the people at the Group of Solid-State Electrochemistry for being great colleagues and friends, and making my time in the group enjoyable and exciting. Particularly, I would like to thank Nalini Vajeeston, Anna Magraso Sola, Vasileios Besikiotis, Harald Fjeld, Tor Svendsen Bjørheim, Liv-Elisif Kalland for their fruitful discussion and sharing of knowledge.

In the second half year of 2012, I was employed in the project of "Dual-CO2". I thank the project leader in UIO Professor Truls Norby for giving me this working opportunity with a very interesting topic and the reliability on me. Furthermore, I am very grateful to colleagues in SINTEF for providing me the working opportunity on the last stage for finishing the Ph.D work.

Finally, I would like to express my deepest thanks to my parents and wife for their endless support and love.

Oslo, March

Wen Xing

Table of Contents

Summary

High-temperature proton and mixed proton-electron conducting materials can be used as electrolytes in fuel cells and as hydrogen separation membranes, respectively. This work contains contributions to the fundamental understanding of the use of ceramic mixed proton-electron conductors in hydrogen separation technologies. Several candidate materials, both single-phase and dual phase (composites), have been characterized with respect to hydrogen permeability and electrical conductivity and the transport properties have been correlated to the structure and defect chemistry of the materials. The reported experimental behavior and comprehension thereof form the bases for evaluation of these specific materials as hydrogen separation membranes. More importantly, it adds to our overall understanding of the processes at play and contributes, as such, to future development of new materials and processes. Five manuscripts comprise the main part of the thesis.

The material screening to uncover single-phase proton conductors in the thesis involves electrical characterizations of three classes of materials; $TiNb_2O_7$, oxides in the La_2O_3-TiO_2 phase diagram and a series of acceptor doped and un-doped gadolinium tungstates (GdWO).

The conductivity of $TiNb_2O_7$ is dominated by electronic conductivity within the present experimental window. There is contribution from proton conductivity as identified by EMF concentration cell measurement, estimated to be ~5% of the total conductivity. It is suggested that hydration of this material occurs by dissolution of water, forming protons and oxygen interstitials charge compensating each other. This is similar to what has been reported for some pyrophosphates [1, 2]. First estimates of the thermodynamic parameters for this hydration process were derived by fitting the suggested defect model to the measured conductivity.

The focus of the investigation of oxides in the La_2O_3-TiO_2 phase diagram was on evaluation of the presence of proton conduction. Proton conduction was observed for acceptor-doped La_2TiO_5, $La_4Ti_9O_{24}$ in this work and for acceptor-doped $La_2Ti_2O_7$ in Ref. [3]. The proton conductivity is, however, much lower than that of state-of-the-art non-perovksite proton conductors, e.g., acceptor doped lanthanum niobate and lanthanum tungstates [4-7] and even more so than the alkaline-earth based cerate and zirconate perovskites [8-14].

For the study of the GdWO series of materials, the aim was to understand effects of acceptor doping and also, by this, adding insight to the relation between the structure and defect chemistry; not only for the specific material under investigation, but also along the series of rare-earth tungstates (LnWO, Ln = rare earths). In GdWO, the dopant solubility was below ~5%, and the maximum proton conductivity was determined to be $2\text{-}3\times10^{-4}$ S/cm. The partial conductivities of oxide ions and electrons were also derived from the conductivity fitting and thermodynamic parameters of hydration and proton migration were extracted. The conductivity analyses show a relatively high ambipolar proton and electron transport giving some promise to use the material as a hydrogen separation membrane. Ordering of the oxygen lattice along the series of rare-earth tungstates with decreasing cation ionic size gives more significant doping effects for the materials with smaller rare-earth, e.g. GdWO and ErWO.

Another major part of this thesis bases on direct hydrogen flux measurement of membrane candidate materials, both as composites and single-phase oxides. The composites investigated comprise $La_{0.995}Ca_{0.005}NbO_{4-\delta}$ and $LaNb_3O_9$, with two different volume ratios, 90:10 and 70:30. $La_{0.995}Ca_{0.005}NbO_{4-\delta}$ and $LaNb_3O_9$ exhibit proton and electron conduction, respectively. The measured hydrogen flux is higher for the 30 vol% $LaNb_3O_9$ composite than for the 10 vol% sample. Limiting factors for the hydrogen flux in both composites are analyzed based on the microstructure and defect chemistry of the membranes. The effect of water splitting on the content of hydrogen in the sweep side at high temperatures is emphasized. The oxide ion conductivity in $La_{0.995}Ca_{0.005}NbO_{4-\delta}$ is estimated based on this effect and compared to that derived from electrical characterization. In addition, the work shows, by way of an example, that the conventional ambipolar transport theory can be applied to dual-phase systems.

The actual hydrogen flux was measured for GdWO as a function of temperature and under various sweep and feed conditions and compared with the hydrogen flux estimated from data of the electrical characterization. The agreement between the flux values derived from the two approaches was satisfactory. As such, this work may serve as a model study illustrating how the hydrogen flux can be predicted/calculated using the data from electrical characterization.

Besides the experimental work stated above, a more theoretical approach is also included in this thesis focusing on doping effects on electrical properties in cation disordered oxides. The self-elimination of doping effect was found and explained based on thermodynamic assessments. The effect of the disorder is partly to offer cation non-stoichiometry to for charge compensating the dopant by site exchange and precipitation of a secondary phase or

micro-domains as an alternative to a mobile anionic defect. The calculation shows that inherent cation disorder reduces significantly the configurational entropy contribution by doping, increasing the Gibbs energy change and thereby decreasing the dopant solubility.

All in all, this thesis involves synthesis, structure analysis, electrical characterization and hydrogen permeation measurements on some of novel candidate materials for proton/mixed conduction. Moderate proton conductivity has been found in most of the investigated materials. The hydrogen flux measurements were performed in the selected single or dual phase systems with relatively high ambipolar conductivity. Based on the experimental work, the elimination of doping effects in cation disordered materials was found and a model describing hydrogen flux and water splitting effect in mixed conducting materials was established. Besides, the possibility of finding good proton conductors with an alternative interstitial type of hydration was discussed with consideration of cation and anion disorder.

1 Introduction

Our society is now experiencing the transition of electricity produced from “hard” and lavish mechanical processes to a “soft” and effective electrochemical process by using fuel cells. High-temperature ionic and electronic conducting oxides are essential for devices in the tantalizing processes related to clean and effective conversion of chemical energy to electricity, e.g., for the electrolyte and electrodes in Solid Oxide Fuel Cells (SOFCs) or as gas separation membranes [15, 16]. Pure ionic conductors are preferred as electrolyte materials and mixed ionic and electronic conductors are the candidates for electrodes in fuel cells and gas separation membranes. Depending on the type of ionic conduction in the electrolyte, SOFCs can be divided into Proton Conducting Fuel Cells (PCFCs) - if the electrolyte is a proton conductor - and the more traditional SOFCs if the electrolyte conducts oxide ions. Mixed proton-electron conductors can serve as hydrogen separation membranes whereas mixed oxide ion-electron conductors can be used for oxygen separation membranes.

Oxides with different structures have been intensively studied with respect to their ionic conduction properties during the last decades. Significant and relatively pure oxide ion conductivity was found in acceptor doped ZrO_2 and CeO_2 based defective fluorites, acceptor doped $LaGaO_3$ based perovskites, and diverse pyrochlore structured oxides [17-21]. These oxides, thus, show great potential to be used as electrolytes in oxide ion conducting SOFCs. Currently, the commercially available high temperature fuel cells are using yttria stabilized ZrO_2 based electrolytes, which in addition to high oxide ion conductivity exhibit excellent chemical and mechanical stability. However, there are still issues with respect to the electrodes physicochemical incompatibility to electrolyte of SOFC, low tolerance to variations in the operating conditions and rather high working temperatures (>750 °C).

In the 1960s, it was realized that oxides dissolve and transport protons in the presence of water vapour or hydrogen gas up to relatively high temperatures, and that proton conducting oxides, as such, may serve as an alternative electrolyte to the conventional oxide ion conductors [22]. Protons are dissolved in the oxides by interaction between the hydrogen containing gas atmospheres and point defects (notably oxygen vacancies) in an exothermic process [23]. State-of-the-art proton conducting oxides comprise a series of alkaline-earth cerates and zirconate perovskites, such as acceptor doped $SrCeO_3$, $BaCeO_3$, $SrZrO_3$ and

$BaZrO_3$ [8, 9, 24]. The proton conductivities for some of these materials are even higher than the oxide ion conductivity in the best oxide ion conductors at temperatures below 700 °C, and the maximum proton conductivity can reach ~5×10^{-2} S/cm. Consequently, PCFCs could potentially have lower operational temperatures than the conventional SOFC. Moreover, the conceptual advantages of PCFCs include higher fuel efficiency and easy water management, since water is produced on the cathode side. Unfortunately, the proton conducting alkaline-earth based perovskites are highly sensitive to acidic gases (e.g., CO_2 and SO_2) [9] and their applications are also hampered by high grain boundary resistance and difficult manufacturing, e.g., Yb doped $BaZrO_3$ (BYZO). Therefore new candidates with both high proton conductivity and good stability under fuel cell operating conditions are continuously being searched for.

In addition, high temperature proton conductivity has been reported for many other groups of oxidic materials, including double perovskites or perovskite-related compounds, rare-earth sesquioxides, rare-earth ortho-niobates and ortho-tantalates, rare-earth tungstates, phosphates and oxidic pycholores [1, 2, 4, 7, 25-31]. The highest proton conductivity among these materials with high stability towards acidic gases was found in un-doped LaWO (La/W=5.3-5.7), in the order of a few mS/cm at temperatures between 600 °C and 900 °C [32]. Still, this is more than one order of magnitude lower than for the best perovskites, and not competitive as a commercial fuel cell electrolyte material unless they are manufactured as membranes with thickness below 5 μm. The search for materials with both high proton conductivity and excellent chemical stability is one important part of this thesis. In this respect, several types of structures with different cation combinations were investigated under different conditions and with different doping strategies emphasizing on the proton conductivity.

Acceptor or donor doping is an effective method used in semiconductors and ionic materials to modify the materials' defect concentrations and obtain the desired electrical or transport properties. However, for some ternary or higher oxides in which two cations with different valences, but similar in size, are disordered, doping may as shown in this thesis lead to negligible or even undesirable effects on functional properties such as the conductivity. Examples comprise $TiNb_2O_7$, TiP_2O_7 and $Ba_3La(PO_4)_3$ [1, 33]. The reason for this absence of doping effects is important to understand material basic properties.

For hydrogen separation applications, there are various types of membrane materials that can be used (e.g., metals, inorganic or organic porous materials and dense ceramics). With emphasis on dense ceramics, both ionic and electronic conduction is equally important which is different from electrolyte materials discussed above. For instance, in the case of hydrogen gas separation membranes, ambipolar electron and proton conduction governs the membrane performance. Mixed conduction for an oxide requires multivalent cations either as part of the parent compound or as dopant. Alternatively one may choose to utilize composite materials consisting of one electron conductor and one proton conductor; i.e. ceramic - metal (cermet) composites or ceramic - ceramic (cercer) composites. In this thesis, both single phase oxides and cercers are investigated with focus on their potentials as hydrogen gas separation membranes. The aim of this work was to increase the understanding of ambipolar transport processes under different conditions and to link the electrical and flux characterization methods, which could enable us to predict membrane performance based on conductivity data alone. In addition, the overall effects of water splitting at high temperatures were evaluated when the membrane conducts three or more charge carriers.

2 Electrical conductivity

Generally, the conductivity of a charged species *i* can be expressed as

$$\sigma_i = z_i e c_i \mu_i \qquad \text{Eq.2.1}$$

where z_i is the absolute charge of the species, e the elementary charge (C), c_i the concentration (cm^{-3}) and μ_i the mobility (cm^2/Vs). In this chapter, the concentration and mobility of the charge carriers of importance to proton and mixed conductors will be discussed.

2.1 Intrinsic defects and doping

The concentration of the charge carriers is determined by the defect structure of the oxide. For stoichiometric ionic conductors, the charge carriers are dominated by intrinsic defects, e.g., Schottky, Frenkel and anti-Frenkel pairs.

By way of example and using the Kröger-Vink notation, the defect reaction describing formation of anti-Frenkel defects is given by:

$$O_O^X = v_O^{\bullet\bullet} + O^{//}, K_{iO} = \frac{[v_O^{\bullet\bullet}][O^{//}]}{[O_O^X]} = \exp(\frac{\Delta S_{af}^0}{R})\exp(\frac{-\Delta H_{af}^0}{RT}) \qquad \text{Eq.2.2}$$

where K_{iO} is the equilibrium constant of the reaction and the terms in square brackets represent the respective defect concentrations in mole fraction. If the oxygen vacancies or interstitials are mobile in the lattice at high temperatures, the oxides will exhibit oxide ion conductivity. The concentration of defects depends on the equilibrium constant which is further determined by the corresponding standard formation entropy and enthalpy, as well as, temperature as shown in Eq. 2.2.

Under sufficiently reducing or oxidizing atmospheres, the defect reaction between native oxygen defects and electronic defects may be significant and they may dominate the electroneutrality condition. The defect reactions are

$$O_O^X = \frac{1}{2}O_2(g) + v_O^{\bullet\bullet} + 2e^{/} \qquad \text{Eq.2.3}$$

for oxygen vacancies and electrons under reducing conditions; and

$$\frac{1}{2}O_2(g) = O_i^{//} + 2h^{\bullet} \qquad \text{Eq.2.4}$$

for oxygen interstitials and holes under oxidizing conditions. Normally, the concentration of intrinsic defects is low (except for highly disordered oxides which will be discussed later), and therefore, the ionic conductivity of un-doped materials is usually rather low. The defect concentration in materials can be modified by aliovalent doping, e.g., as mentioned above, acceptor doped ZrO_2 (YSZ) and CeO_2 for oxide ion conductors, and acceptor doped $LaNbO_4$ and $BaZrO_3$ for proton conductors [6, 21, 34]. Acceptor doping is utilized to increase the concentration of oxygen vacancies, thus giving rise to higher oxide ion conduction and in turn proton conduction when the vacancies are hydrated under wet conditions. The hydration processes will be treated in the following section.

Acceptor-doping in general results in formation of oxygen vacancies and the electroneutrality condition is dominated by the two defects under certain conditions:

$$2[v_O^{\bullet\bullet}] = [A^{/}] \qquad \text{Eq.2.5}$$

The concentration of oxygen vacancies increases with increasing dopant concentration until the dopant reaches its solubility limit in the host oxides. However, at a certain dopant concentration, the defects may start to interact with each other forming defect associates and the material's conductivity levels off or even decreases upon further increase in the dopant concentration. Examples of defect association has, among others, been reported for acceptor doped ZrO_2, CeO_2 and $LaNbO_4$ [34-36].

Although the doping strategy has been successful in many materials to modify electrical properties, it may fail in materials with highly disordered cation or anion sub-lattices. In this group of materials the large amounts of intrinsic defects dominate and serve as a "buffer" to eliminate effects of aliovalent doping. This has been explored in detail in Manuscript I.

2.2 Hydration and proton concentration

Under hydrogen containing conditions, hydride ions [37] and/or protons may form in the crystal structure of oxides by different reactions. Protons are the most abundant hydrogen defects, residing in the electron cloud of negatively charged oxide ions. Since protons in oxides are effectively positively charged, either annihilation of other positive defects or creation of negative defects must follow hydration to retain electroneutrality. We will discuss different possible routes for hydration in the following sub-sections.

2.2.1 Hydration of oxygen vacancies

Hydration of oxygen vacancies forming protons can be expressed as follows:

$$H_2O(g) + v_O^{\bullet\bullet} + O_O^X = 2OH_O^{\bullet} \qquad \text{Eq.2.6}$$

This is the reaction most commonly encountered in oxides with oxygen vacancies as predominant native defects. The amount of protons therefore highly depends on the available amount of oxygen vacancies for hydration. As discussed above, the oxygen vacancy concentration can be increased by acceptor doping. Some classes of materials, for instance, perovskite oxides (with the general formula ABO_3), can accommodate rather high concentration levels of aliovalent cations substituted for the parent cations, in the order of a few tens of mole percent [38]. For other classes of materials, the solubility limit of the dopant is far lower, e.g., below 1% in $LaNbO_4$ and 5% in Gd_6WO_{12}.

In an acceptor doped system where protons are one of the majority defects, the electroneutrality can be written as:

$$[A^{/}] = 2[v_O^{\bullet\bullet}] + [OH_O^{\bullet}] \qquad \text{Eq.2.7}$$

The concentrations of protons and oxygen vacancies under different conditions depend on the thermodynamics of the hydration reaction (reaction in Eq. 2.6):

$$K_v = \frac{[OH_O^{\bullet}]^2}{[v_O^{\bullet\bullet}]p_{H_2O}[O_O^X]} = \exp\frac{-\Delta G_v^0}{RT} = \exp\frac{\Delta S_v^0}{R}\exp\frac{-\Delta H_v^0}{RT} \qquad \text{Eq.2.8}$$

The proton concentration can in this case be derived by inserting Eq.2.7 into Eq.2.8 and solving the resulted quadratic equation. For two of the materials investigated in this thesis, acceptor doped Gd_6WO_{12} and La_2TiO_5, the proton concentration in the acceptor doped composition was calculated through the solution to the above set of equations.

For the hydration thermodynamics, the molar entropy change of the hydration reaction is believed to be dominated by the consumption of one mole of water vapor with ~ -120 J/molK [39].

In general for proton conductors, the value of standard molar hydration enthalpy is negative, ranging from approximately -20 kJ/mol to -200 kJ/mol [40]. These exothermic enthalpies imply that protons dominate at low temperatures and oxygen vacancies at high temperatures. The hydration enthalpy can be extracted from thermogravimetry (TG) and conductivity measurements by fitting defect chemistry models to the measured data, and determined directly by combined TG and Differential Scanning Calorimetry (DSC). Some apparent correlations between the hydration enthalpy and material properties have been sought for acceptor doped perovskites [23, 40]. Figure 1 shows, by way of example, the calculated proton concentration as a function of temperature with different hydration enthalpies in a 2% acceptor doped oxide.

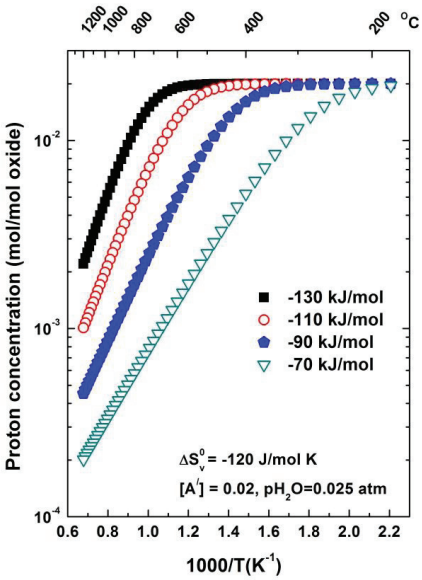

Figure 1: Proton concentration as a function of inverse absolute temperature with different hydration enthalpies for vacancy type of hydration

As mentioned above, intrinsic defects can dominate in anion-disordered oxides. These inherent oxygen vacancies can also be hydrated giving proton conductivity. When the oxide

ions are randomly distributed on the anion sub-lattices, an average ideal charge can be assigned to the regular oxygen sites, generally slightly smaller than the integer -2. Consequently, the oxide ion on an oxygen site would have an effectively negative charge which is compensated by positively charged oxygen vacancies. One may derive a nomenclature with corresponding defect reaction and thermodynamics for systems with anion disordered oxide, e.g., "La_6WO_{12}" and $Ca_{12}Al_{14}O_{33}$ [41-43].

In this work, hydration of acceptor doped Gd_6WO_{12}, and acceptor doped oxides in the La_2O_3-TiO_2 phase diagram follows Eq. 2.6. However, the electrical and phase investigation on $TiNb_2O_7$ revealed that an alternative hydration process may occur, which will be discussed in the following paragraphs.

2.2.2 Alternative hydration reaction

Hydration or protonation with simultaneous formation of oxygen interstitials charge compensating the protons can be expressed by Eq. 2.9:

$$H_2O(g) + 2O_O^X = 2OH_O^\bullet + O_i'' \qquad \text{Eq.2.9}$$

with the equilibrium constant:

$$K_i = \frac{[OH_O^\bullet]^2[O_i'']}{[O_O^X]p_{H_2O}} = \exp\frac{-\Delta G_i^0}{RT} = \exp\frac{\Delta S_i^0}{R}\exp\frac{-\Delta H_i^0}{RT} \qquad \text{Eq.2.10}$$

Hydration following this route may be found in oxides prone to accommodate oxygen interstitials.

If protons and oxygen interstitials are the majority defects through the above hydration reaction, the electroneutrality yields:

$$[OH_O^\bullet] = 2[O_i''] \qquad \text{Eq.2.11}$$

Their concentration can be derived through Eqs. 2.10 and 2.11:

$$[OH_O^\bullet] = 2[O_i''] = 2^{\frac{1}{3}}K_i^{\frac{1}{3}}pH_2O^{\frac{1}{3}} \qquad \text{Eq.2.12}$$

For doped materials, e.g., the intrinsically donor-doped $TiNb_2O_7$ induced by Nb over-stoichiometry, the electroneutrality condition involves the concentration of donors and can, accordingly, be written as:

$$[OH_O^{\bullet}] + [D^{\bullet}] = 2[O_i^{//}] \qquad \text{Eq.2.13}$$

By combining Eq.2.10 and Eq.2.13, a cubic equation can be obtained and the proton concentration can be expressed as

$$[OH_O^{\bullet}] = 2[O_i^{"}] - [D^{\bullet}] = \frac{1}{3}\left(-[D^{\bullet}]^3 + 27K_i p_{H_2O} + 3\sqrt{-6[D^{\bullet}]^3 K_i p_{H_2O} + 81K_i^2 p_{H_2O}^2}\right)^{1/3} + \qquad \text{Eq.2.14}$$

$$\frac{[D^{\bullet}]^2}{3\left(-[D^{\bullet}]^3 + 27K_i p_{H_2O} + 3\sqrt{-6[D^{\bullet}]^3 K_i p_{H_2O} + 81K_i^2 p_{H_2O}^2}\right)^{1/3}} - \frac{2}{3}[D^{\bullet}]$$

The calculated proton concentration as a function of inverse temperature in a donor doped system with different values of the hydration enthalpy is shown in Figure 2. For the sake of demonstration, the concentration of oxygen interstitials is assumed to be unlimited, which is not the case for real systems.

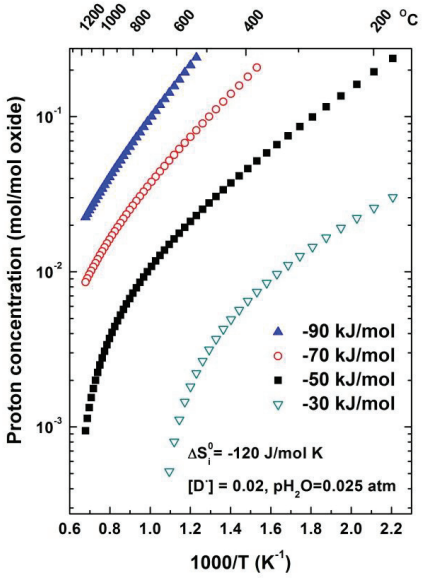

Figure 2: Proton concentration as a function of inverse absolute temperature with different hydration enthalpies for interstitial type of hydration

For acceptor doped material, the acceptors would create positive defects such as oxygen vacancies. If we further assume that these oxygen vacancies are fully consumed by hydration at high water vapor pressure, then the electroneutrality condition changes to:

$$[OH_O^{\bullet}] = 2[O_i^{//}] + [A^{/}] \qquad \text{Eq.2.15}$$

The proton concentration can be obtained by inserting the above electroneutrality equation into Eq. 2.10 and solving another cubic equation.

As compared to the proton concentration in the acceptor doped system where the maximum concentration is determined by the concentration of acceptors, the limitation of maximum proton concentration for materials with interstitial type hydration would be determined by the oxygen interstitials tolerance in the structure which will be further interpreted in the Discussion of the thesis.

2.3 Proton conductivity

The above section describes the formation and concentration of protons by different routes dissolved from water vapor. Another important parameter that governs the proton conductivity is its mobility and by assuming that proton transport is an activated process, the mobility can be expressed as

$$\mu_i = \mu_{0,i} \frac{1}{T} \exp\left(\frac{-\Delta H_{mob,i}}{RT}\right) \qquad \text{Eq.2.16}$$

where $\mu_{0,i}$ is the pre-exponential factor of charge mobility (cm^2K/Vs) and $\Delta H_{mob,i}$ the enthalpy of migration.

The pre-exponential term $\mu_{0,i}$ can be expanded into

$$\mu_{0,i} = \Gamma_{0,i} \alpha s^2 \frac{zF}{R} \exp\left(\frac{\Delta S_{mob}}{R}\right) \qquad \text{Eq.2.17}$$

where $\Gamma_{0,i}$ is the attempt frequency, α is the structure parameter, s is the average jump distance and ΔS_{mob} is the entropy of mobility. Within one type of diffusion mechanism and especially for materials with similar structure, the variations of $\mu_{0,i}$ are rather small.

Based on modelled parameters and the equations derived for hydration of acceptor and donor doped materials it would be interesting to see how the different thermodynamic and transport parameters influence the overall proton conductivity. Figure 3a and b therefore present the temperature dependence of the proton conductivity for the two hydration routes with different physicochemical parameters.

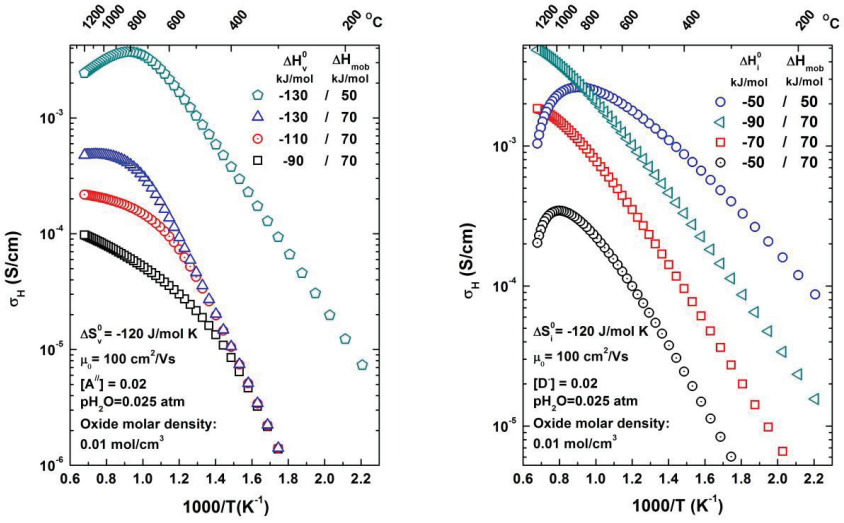

Figure 3: Modelled proton conductivity as a function of inverse absolute temperatures for vacancy (left) and interstitial (right) types of hydration processes with different parameters.

By comparing the two simulated conductivities for vacancy and interstitial types of hydration, we see that both types have maximum proton conductivities at high temperatures with our preset parameters. However, the conductivity bends more significantly at high temperatures for interstitial type of hydration with less negative hydration enthalpy value in a donor doped system than for the vacancy type of hydration by keeping the same assumed proton mobility. This reflects the significant difference in the two types of hydration thermodynamics as stated in the above section describing the proton concentration.

3 Ambipolar transport and hydrogen flux

Ambipolar transport theory is essential for studying dense ceramic mixed conducting membranes. Several experimental and modelling studies have been performed on hydrogen and oxygen transport in both single and multiphase ceramic membranes during the past decades, e.g. in refs. [43-46]. In this section, we will discuss the equations describing the processes governing hydrogen transport in a membrane exposed to chemical potential gradients. The analyses are mostly based on ref. [16] and provide an overview of the transport theory relevant to hydrogen and oxygen fluxes in mixed conducting materials under different defect chemical conditions. They will, as such, provide the theoretical background and make it easier to follow the more brief descriptions in the papers.

Based on Wagner type transport theory it follows that when a force (expressed by the negative gradient in a potential P_i) is applied on a species, i, a flux of the species can be generated. The one-dimensional expression for the flux density can be written as:

$$j_i = B_i\, c_i \frac{-dP_i}{dx} \qquad \text{Eq.3.1}$$

where B_i is the mechanical mobility of species i and c_i is the concentration of the species. In the case of an electrochemical potential, η_i, the above expression becomes:

$$j_i = B_i\, c_i \frac{-d\eta_i}{dx} = -B_i\, c_i \left[\frac{d\mu_i}{dx} + z_i F \frac{d\varphi}{dx}\right] \qquad \text{Eq.3.2}$$

where μ_i and φ represent the chemical potential and electrical potential, and z_i and F are the charge of the species and Faraday constant, respectively. The mechanical mobility for charged species can be replaced by the conductivity yielding:

$$j_i = \frac{-\sigma_i}{(z_i F)^2}\left[\frac{d\mu_i}{dx} + z_i F \frac{d\varphi}{dx}\right] \qquad \text{Eq.3.3}$$

The flux density for the species i gives rise to a partial current density and under open circuit conditions the sum of the partial current densities in a membrane over all the species, k, is zero:

$$i_{tot} = \sum_k z_k F j_k = -\sum_k \frac{\sigma_k}{z_k F}\left[\frac{d\mu_k}{dx} + z_k F \frac{d\varphi}{dx}\right] = 0 \qquad \text{Eq.3.4}$$

The expression for the electrical potential gradient through the sample in terms of the transport number and chemical potential gradient of all charge carriers can be derived by using the definition of transport number, $t_k = \frac{\sigma_k}{\sigma_{tot}} = \frac{\sigma_k}{\sum_k \sigma_k}$, and we obtain:

$$\frac{d\varphi}{dx} = -\sum_k \frac{t_k}{z_k F}\frac{d\mu_k}{dx} \qquad \text{Eq.3.5}$$

By inserting Eq. 3.5 into Eq. 3.3, we obtain a general expression which can be used to calculate the flux of a particular charged species:

$$j_i = \frac{-\sigma_i}{(z_i F)^2}\left[\frac{d\mu_i}{dx} - z_i \sum_k \frac{t_k}{z_k}\frac{d\mu_k}{dx}\right] \qquad \text{Eq.3.6}$$

Under steady state (constant flux density everywhere), the integration over the thickness of the membrane, L, gives:

$$j_i = \frac{-1}{(z_i F)^2 L}\int_I^{II} \sigma_i \left[d\mu_i - z_i \sum_k \frac{t_k}{z_k} d\mu_k\right] \qquad \text{Eq.3.7}$$

The chemical potential of the charged species can be related to their neutral counterparts through:

$$d\mu_{E^z} = d\mu_E - z d\mu_{e^-} \qquad \text{Eq.3.8}$$

where E refers to a neutral chemical entity, *z* can be positive or negative, and e^- represents an electron. The chemical potential gradients can be expressed in terms of activities, and/or in terms of partial pressures assuming isothermal conditions and ideal gases:

$$d\mu_E = RT d\ln a_E = RT d\ln p_E \qquad \text{Eq.3.9}$$

By inserting the chemical potentials of neutral species and rearranging, the flux density of *i* among all ions n, can be given as:

$$j_i = \frac{-1}{(z_i F)^2 L}\int_I^{II} \sigma_i \left[d\mu_{n=i} - z_i \sum_n \frac{t_n}{z_n} d\mu_n\right] \qquad \text{Eq.3.10}$$

with $\mu_{n=i}$ and μ_n being the chemical potentials of the corresponding neutral species.

From Eq. 3.10, the flux of protons (species i) in a mixed proton, oxide ion and electron conductor with hydrogen and oxygen as neutral species, can be expressed as:

$$j_{H^+} = \frac{-RT}{4F^2L}\int_{I}^{II}\sigma_{H^+}\left[2(t_{O^{2-}}+t_{e^-})d\ln p_{H_2(g)} + t_{O^{2-}}\,d\ln p_{O_2(g)}\right] \qquad \text{Eq.3.11}$$

Proton transport through the membrane can be in the form of hydrogen and/or water. When the membrane material conducts predominantly protons and electrons, Eq. 3.11 can be simplified to:

$$j_{H^+} = \frac{-RT}{2F^2L}\int_{I}^{II}\sigma_{H^+}\,t_{e^-}\,d\ln p_{H_2(g)} \qquad \text{Eq.3.12}$$

The term $\sigma_{H^+}\,t_{e^-}$ in the above equation can be rearranged by the definition of transport number to:

$$\sigma_{H^+}\,t_{e^-} = \sigma_{total}\,t_{H^+}\,t_{e^-} = \sigma_{e^-}\,t_{H^+} = \frac{\sigma_{H^+}\sigma_{e^-}}{\sigma_{total}} \qquad \text{Eq.3.13}$$

$\frac{\sigma_{H^+}\sigma_{e^-}}{\sigma_{total}}$ is the so-called ambipolar proton-electron conductivity.

In the case that electronic conduction predominates ($t_{e^-} \approx 1$), proton conductivity is the limiting factor for the proton flux. In the following part, we will discuss the integration of Eq. 3.12 under different limiting situations with respect to the materials defect chemistry.

If protons are minority defects, then their concentration and, consequently, the proton conductivity is proportional to $p_{H_2}^{1/2}$, and we obtain (3.14):

$$j_{H^+} = \frac{-RT\sigma_{H^+,0}}{2F^2L}\int_{I}^{II}p_{H_2(g)}^{1/2}d\ln p_{H_2(g)} = \frac{-RT\sigma_{H^+,0}}{F^2L}\left[\left(p_{H_2(g)}^{1/2}\right)^{II} - \left(p_{H_2(g)}^{1/2}\right)^{I}\right] \qquad \text{Eq.3.14}$$

Here $\sigma_{H^+,0}$ is the proton conductivity at standard hydrogen pressure (1 atm H_2(g)). If protons are majority defects and compensated by electrons, their concentration and thereby the proton conductivity are proportional to $p_{H_2}^{1/4}$, and we obtain:

$$j_{H^+} = \frac{-RT\sigma_{H^+,0}}{2F^2L}\int_{I}^{II}p_{H_2(g)}^{1/4}d\ln p_{H_2(g)} = \frac{-2RT\sigma_{H^+,0}}{F^2L}\left[\left(p_{H_2(g)}^{1/4}\right)^{II} - \left(p_{H_2(g)}^{1/4}\right)^{I}\right] \qquad \text{Eq.3.15}$$

If protons are majority defects and compensated by acceptor-dopants, then their concentration and the proton conductivity are independent of p_{H_2}, and we obtain:

$$j_{H^+} = \frac{-RT\sigma_{H^+}}{2F^2L}\int_I^{II} d\ln p_{H_2(g)} = \frac{-RT\sigma_{H^+}}{2F^2L}\int_I^{II}\frac{1}{p_{H_2(g)}}dp_{H_2(g)} = \frac{-RT\sigma_{H^+}}{2F^2L}\left[\ln p_{H_2(g)}{}^{II} - \ln p_{H_2(g)}{}^{I}\right] \qquad \text{Eq.3.16}$$

If the transport number of protons is unity we may write:

$$j_{H^+} = \frac{-RT}{2F^2L}\int_I^{II}\sigma_{H^+}\, t_{e^-}\, d\ln p_{H_2(g)} = \frac{-RT}{2F^2L}\int_I^{II}\sigma_{e^-}\, t_{H^+}\, d\ln p_{H_2(g)} = \frac{-RT}{2F^2L}\int_I^{II}\sigma_{e^-} d\ln p_{H_2(g)} \qquad \text{Eq.3.17}$$

If protons compensate the acceptors, then the electronic conductivity is proportional to $p_{H_2}^{1/2}$ and $p_{H_2}^{-1/2}$, respectively, in the case of electrons (n-type) and holes (p-type) if p_{O_2} is assumed constant. This gives:

$$j_{H^+} = \frac{-RT\sigma_{n,0}}{2F^2L}\int_I^{II} p_{H_2}^{1/2} d\ln p_{H_2(g)} = \frac{-RT\sigma_{n,0}}{2F^2L}\int_I^{II} p_{H_2}^{-1/2} dp_{H_2(g)} = \frac{-RT\sigma_{n,0}}{F^2L}\left[\left(p_{H_2}^{1/2}\right)^{II} - \left(p_{H_2}^{1/2}\right)^{I}\right] \qquad \text{Eq.3.18}$$

for limiting n-type conductivity, and

$$j_{H^+} = \frac{-RT\sigma_{p,0}}{2F^2L}\int_I^{II} p_{H_2}^{-1/2} d\ln p_{H_2(g)} = \frac{-RT\sigma_{p,0}}{2F^2L}\int_I^{II} p_{H_2}^{-3/2} dp_{H_2(g)} = \frac{RT\sigma_{p,0}}{F^2L}\left[\left(p_{H_2}^{-1/2}\right)^{II} - \left(p_{H_2}^{-1/2}\right)^{I}\right] \qquad \text{Eq.3.19}$$

for limiting p-type conductivity. σ_n and σ_p are electron and hole conductivities, respectively, and $\sigma_{n,0}$ and $\sigma_{p,0}$ are conductivities at standard hydrogen pressure (1 atm $H_2(g)$).

The proton flux in mixed conductors has been discussed above. Whether the overall transport across the membranes yields permeation of hydrogen and/or water really depends on the details of the conduction properties of the material and the chemical potential gradient across it. In addition, it is important to recognize that for materials with mixed electron and oxide ion conductivity, effects of water splitting must be taken into account for flux measurements under wet sweep conditions when evaluating the concentration of different gaseous species in the outlet of the permeate side. The magnitude of the water splitting is determined by the ambipolar oxide ion and electronic conduction induced by the gradient in the oxygen partial pressure from the sweep to the feed side of the membrane according to:

$$j_{H_2}^{H_2O} = j_{O^{2-}} = \frac{RT}{8F^2L}\int_I^{II}\frac{\sigma_{O^{2-}}\sigma_{e^-}}{\sigma_{H^+} + \sigma_{e^-} + \sigma_{O^{2-}}} d\ln p_{O_2} \qquad \text{Eq.3.20}$$

One should be aware of the water splitting when interpreting the measurement data to make appropriate application design in membrane reactor. This will be discussed in Discussion part.The effects of water splitting on the overall measured hydrogen concentration in the sweep side are discussed in detail in two of the manuscripts in this work.

Composites can be used in membrane science to utilise the specific transport properties of each phase in the membrane. In the present thesis the electronic conductor $LaNb_3O_9$ was mixed with proton conducting acceptor-doped $LaNbO_4$ to obtain high ambipolar proton-electron conductivity. The conventional ambipolar transport theory derived above was applied where the transport is dominated by the materials bulk property. However, since the complexity of the microstructure of composites will influence the transport properties, additional considerations (e.g., sample microstructure, percolation situation) must be taken when equations derived for single phase materials are applied.

As the membrane becomes sufficiently thin, surface kinetics will become important [47] and diffusion of protons across the membrane will no longer be rate determining for the overall hydrogen flux. Composites could be more vulnerable towards slow surface kinetics as the reactions at the surface may require triple-phase-boundaries between the proton and the electron conductors and the gas phase. Since the hydrogen flux were determined only by bulk transport properties in all the samples investigated in this work, therefore, we will not treat surface kinetics in detail.

4 Experimental methods

This chapter presents details of the experimental methods which are employed for the characterization of the transport properties of the oxides in this thesis. The chapter will focus on the gas controlling system and impedance spectroscopy, both of which are important but less described in the attached manuscripts. The other aspects of the applied experimental methods in this thesis (e.g., synthesis, structure and electrical characterizations), have already been described in detail in separated papers.

4.1 Gas mixer

An in-house-built gas mixer [48] is used to control the atmosphere during conductivity and hydrogen flux measurements. A schematic illustration of the gas mixer is shown in Fig.4. It contains a series of flowmeters (Sho-rate 1355, Brooks Instrument) mounted in pairs, with different floaters of either glass or Ta. The different oxygen partial pressures are achieved by diluting pure oxygen or hydrogen (G1) with argon (G2) in three stages. The two gases are introduced into the gas mixer by flowmeter G1 and G2, and the mixture between the two (M1) can then be further diluted with G2 (Ar) yielding the second mixture (M2) that is then fed into the third mixing stage (flowmeter pair, M3) to be diluted once more. The gas can be diluted in a ratio of about 1:30 when the heavier tantalum ball is used in the flowmeter for inert gas. Each pairs of flowmeters are connected to a bubbler (glass column, B1-B4) filled with dibutylphtalate. The purpose of the bubbler is to let the spare gas out and to ensure that the over-pressure of the gases in the mixer is not too high. The over-pressure decreases along the mixing stages, by having shorter bubblers, to "push" the gas in the intended direction.

The water partial pressure is controlled by mixing wet and dry gases from M3 in the fourth flowmeter pair (M4) after passing M3 either through a solution of distilled water saturated with potassium bromide (KBr) or phosphorus pentoxide (P_2O_5); the wetting or drying stages, respectively. The pH_2O of the gas after passing through a saturated KBr solution yields a water content of 2.5% at 25 °C. Similarly, D_2O wetting stages yield a slightly lower pD_2O [49].

For pH_2O control in reducing atmosphere, the oxygen partial pressure was kept constant by first bubbling H_2 through the wetting stage and then diluting the wet H_2 with inert gas (Ar), keeping the ratio between the hydrogen and water vapour constant. For hydrogen flux

measurement, the feed side was controlled by the first four pairs of flowmeters and the sweep side was controlled by the last two pairs with Ar chosen as G3.

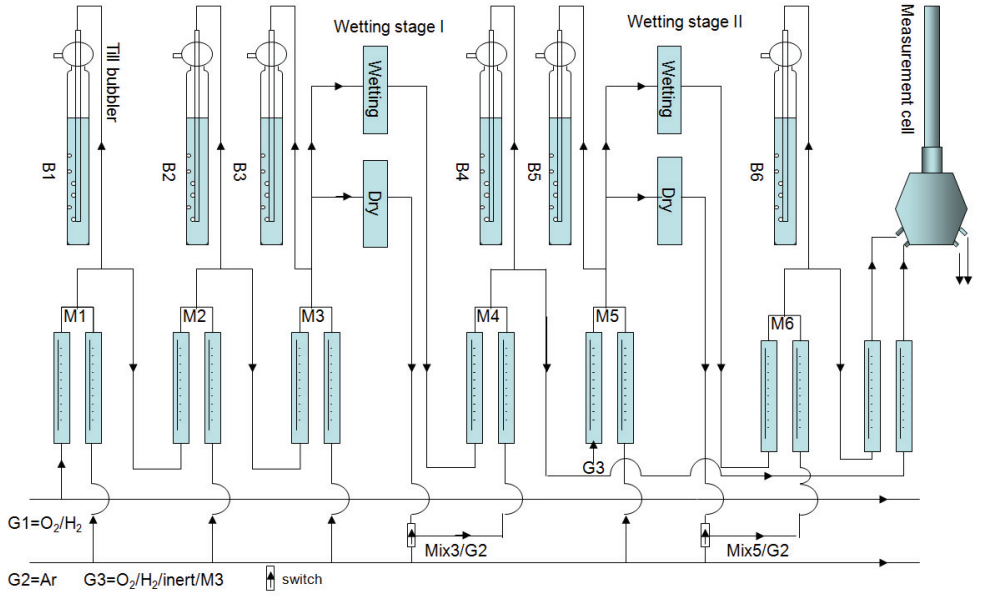

Figure 4: *Schematic illustration of the gas mixer unit used for the conductivity measurements and hydrogen flux measurements.*

4.2 Flux measurements

All hydrogen flux measurements in this work were conducted in a ProboStat™ cell (NorECs, Norway) with an outer enclosing alumina tube and an inner support tube of alumina. Sealing was achieved by using a gold gasket between the membrane and the inner support tube with an applied spring force on top of the membrane. The membrane was sealed to the alumina support tube at approximately 1050 °C. The gas compositions were controlled by the gas mixer supplying pure hydrogen, 10% hydrogen in helium, and mixtures of hydrogen and argon as feed gas, and wet or dry argon as sweep gas.

The sweep gas was analyzed in a 3000 Plus Agilent Micro-Gas Chromatograph (GC). The sealing was monitored by detecting the leakage of helium (feed) in argon (sweep), reaching helium contents below the detection limit of the GC (< 1 ppm) in most cases and a few ppm for the worst case. The leakage was accounted for during calculation of the hydrogen flux by assuming the same leakage rate for hydrogen as for helium, and it was always below 5% of

the total hydrogen flux. Hydrogen flux through the alumina tube at these temperatures is negligible due to low electronic and ionic transport.

4.3 Impedance spectroscopy

Impedance spectroscopy plays an important role in distinguishing transport through "specimen elements" with different time constants, e.g., bulk and grain boundary. It uses alternating current (AC) to measure the complex impedance of a sample over a broad frequency range, from typically a few MHz to a few mHz.

In the present work, it is assumed that the sample microstructure consists of cubic grains with grain boundaries in between according to the Brick-Layer model [50]. The grain interior and grain boundary are represented by the first two (RQ) semi-circles $(R_1Q_1)(R_2Q_2)$ in the Nyquist type of spectra plotting, where the (RQ) corresponds to a parallel circuit consisting of a resistor (R) and a constant phase element (CPE, the Q). The specific grain interior and grain boundary conductivity can be determined from the resistances associated with the different semicircles and the width of grain interior and grain boundary:

$$\sigma_{gi} = \frac{1}{R_1} \qquad \text{Eq. 4.1}$$

and

$$\sigma_{gb} = \frac{g}{G}\frac{1}{R_2} \qquad \text{Eq. 4.2}$$

Here G and g denote the grain interior and grain boundary thicknesses, respectively.

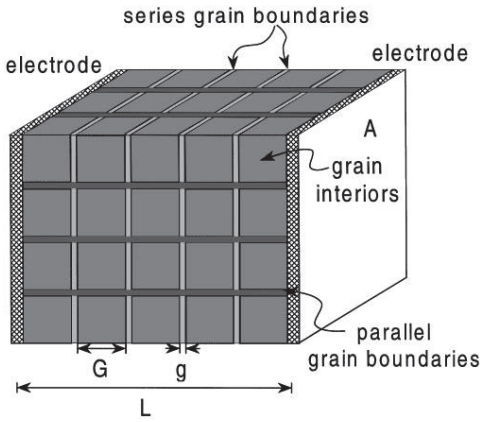

Figure 5: Illustration of brick layer model from [50]. The grain interior is represented by the cubic-shape and grain boundaries exist as flat layers between the cubes. The size of the two parts is denoted by g and G.

The impedance spectra were fitted to the model circuits by applying the "Equivalent circuit for Windows" software. The observed semicircles were deconvoluted to resistances (R), Y and n which are the parameters for describing the CPE. The quasi-equivalent capacitance of a parallel circuit consisting of a resistor and CPE can be calculated by the following expression:

$$C = Y^{1/n} R^{(1-n)/n} \qquad \text{Eq. 4.3}$$

Based on the calculated capacitances, we could adjust the measuring frequency of our constant frequency electrical measurements to ensure that the materials grain interior property was measured since the material grain interior property is the focus of this thesis.

5 Manuscripts

Manuscript I

Title: Effect of cation disorder on the solubility and result of doping in oxides
Authors: Wen Xing, Kazuaki Toyoura, Truls Norby
Status: Published in International Journal of Hydrogen Energy

Manuscript II

Title: Hydrogen permeation, transport properties and microstructure of Ca-doped $LaNbO_4$ and $LaNb_3O_9$ composites
Authors: Wen Xing, Guttorm E. Syvertsen, Tor Grande, Zuoan Li, Reidar Haugsrud
Status: Published in Journal of Membrane Science

Manuscript III

Title: Structure and transport properties in un-doped and acceptor-doped Gadolinium Tungstate
Authors: Wen Xing, Protima Rauwel, Charles H. Hervoches, Zuoan Li, and Reidar Haugsrud
Status: Submitted to Journal of Membrane Science

Manuscript IV

Title: Defects and transport properties in $TiNb_2O_7$
Authors: Wen Xing, Liv-Elisif Kalland, Zuoan Li, and Reidar Haugsrud
Status: Submitted to Journal of American Ceramic Society

Manuscript V

Title: Electrical characterization of compounds with different structures in La_2O_3-TiO_2 phase diagram
Authors: Wen Xing
Status: Manuscript

Publication during Ph.D not included in the thesis

Title: High Temperature Proton Conductivity of ZrP_2O_7
Authors: Nalini Vajeeston, Koji Amezawa, Wen Xing and Truls Norby
Status: Published in Journal of the Electrochemical Society

I

Manuscript I

Effect of cation disorder on the solubility and result of doping in oxides

Wen Xing, Kazuaki Toyoura, Truls Norby

International journal of hydrogen energy, ISSN 0360-3199. **37(9)**, s 8062- 8065

doi: 10.1016/j.ijhydene.2011.11.136

II

Manuscript II

Hydrogen permeation, transport properties and microstructure of Ca-doped $LaNbO_4$ and $LaNb_3O_9$ composites

Wen Xing, Guttorm E. Syvertsen, Tor Grande, Zuoan Li, Reidar Haugsrud

Journal of Membrane Science, ISSN 0376-7388. **415**, s 878- 885

doi: 10.1016/j.memsci.2012.06.008

III

Manuscript III

Structure and transport properties in un-doped and acceptor-doped Gadolinium Tungstate

Wen Xing, Protima Rauwel, Charles H. Hervoches, Zuoan Li, Reidar Haugsrud

Submitted to *Journal of Membrane Science*

Manuscript IV

Defects and transport properties in $TiNb_2O_7$

Wen Xing, Liv-Elisif Kalland, Zuoan Li, and Reidar Haugsrud

Submitted to *Journal of American Ceramic Society*

IV

Defects and transport properties in $TiNb_2O_7$

Wen Xing, Liv-Elisif Kalland, Zuoan Li, and Reidar Haugsrud [z]

Department of Chemistry, University of Oslo, Centre for Materials Science and Nanotechnology, FERMiO, Gaustadalleen 21, NO-0349 Oslo, Norway

Abstract

The electrical conductivity of $TiNb_2O_7$ was characterized as a function of temperature, p_{O_2} and p_{H_2O}. The total conductivity was independent of p_{O_2} in the low oxygen partial pressure regime, while a dependency of $p_{O_2}^{-1/4}$ was observed at higher oxygen partial pressures. The conductivity increased with increasing p_{H_2O} under oxidizing conditions below 700 °C. Mixed electronic and protonic conduction was indicated by H/D isotope exchange and transport number measurements. A defect model based on interstitial type of hydration was established and fitted to the conductivity data allowing for determination of physicochemical parameters of hydration and electron migration.

Keywords: $TiNb_2O_7$; defect chemistry; conductivity; hydration

[z] E-mail: reidar.haugsrud@smn.uio.no

1. Introduction

High-temperature proton conducting oxides have received increasing interest since appreciable proton conductivity was reported for perovskites such as acceptor doped $SrCeO_3$ in the early 1980s [1]. Besides the perovskite structured oxides, several new classes of proton conductors were uncovered during the last 10 years, where examples include rare-earth tungstates and rare-earth ortho-niobates, and oxysalts like the rare-earth phosphates [2-7]. Among phosphates, pyrophosphates such as TiP_2O_7 and ZrP_2O_7 were also reported to be proton conductors under wet conditions [8-10].

Depending on the detailed transport properties, proton conducting ceramics may serve as the functional component of membranes for hydrogen separation and as electrodes or electrolytes for Proton Conducting Fuel Cells (PCFCs) [11]. In a dense ceramic hydrogen separation membrane, mixed proton-electron conductivity is a prerequisite, since the hydrogen flux is governed by the so-called ambipolar proton-electron conductivity, assuming fast surface kinetics [12]. In most cases, mixed conduction can be found in proton conductors constituting reducible parent cations [13].

In this work, mixed ionic-electronic conductivity of $TiNb_2O_7$ has been addressed and characterized as a function of temperature, oxygen partial pressure, p_{O_2}, and water vapor partial pressure, p_{H_2O}. Isotope effect (H_2O/D_2O) and transport number measurements were conducted to identify the contribution of protons to the overall conductivity. The results are rationalized in terms of point defect chemistry and transport models.

2. Experimental

Nominal $TiNb_2O_7$ was prepared by mixing titanium (IV) oxide (Alfa Aesar, 99.5%) and niobium (V) oxide (Alfa Aesar, 99.9%), followed by heat treatment at 800 °C for 1 hour. The powder was milled in an agate mortar and pressed isostatically into green tablets that afterwards were sintered at 1250 °C for 5 hours.

A FEG-SEM Quanta 200F Scanning Electron Microscope (SEM) with an energy dispersive X-ray spectrometer (EDS) was used to examine the grain size, morphology and chemical composition of the sintered ceramics. Moreover, the structure and phase-purity were studied by X-ray diffraction using a Siemens D-5000 diffractometer with Cu Kα radiation.

Electrical conductivity measurements and impedance spectroscopy were performed by mounting the specimens in a ProboStat™ cell (NorECs, Norway) and using a standard two electrode-four wire setup with Pt paint and mesh as electrodes on the sample surfaces. The total conductivity was measured at a constant frequency of 10 kHz with an oscillation voltage of 1.1V rms using an HP 4192A impedance analyzer. Impedance spectroscopy was conducted in the frequency range from 5 to 10^6 Hz yielding one semicircle in a Nyquist plot that was fitted to a (RQ) model circuit by means of the Equivalent Circuit for Windows software. The fitted capacitance showed that the resistances derived from the semicircle correspond to grain interior. Due to the relatively high conductivity under reducing conditions, a 4-point electrode setup (van der Pauw method) was used in hydrogen containing atmospheres. For transport number measurements, a 1 mm thick gold gasket was placed between the specimen and the alumina support tube. After heating to ~1060 ºC to soften the gold, the specimen separates two gas volumes; one in the inner compartment inside the support tube and the other in the volume enclosed by the outer, closed-end alumina tube. Well-defined oxygen partial pressure, p_{O_2}, and water vapor partial pressures, p_{H_2O}, for the

isothermal partial pressure dependences, as well as, for the gradients in the transport number measurements were established by mixing oxygen, argon and water vapor under oxidizing conditions and hydrogen, argon and water under reducing conditions. Details of the gas mixer can be found in Ref. [14].

3. Results

3.1 Structure and sample characterization

The grain size of the sintered sample ranges from 2 to 10 μm as shown by the SEM pictures in Fig. 1. A secondary phase is observed by the phase contrast of the back scattered electron image (cf. Fig. 1(b)), and it was shown by EDS analyses to be titanium-rich. Based on this, we anticipate that the bulk material is over-stoichiometric with respect to Nb. This was confirmed by Electron Probe Micro Analysis showing that the bulk material has a ~2% excess of Nb.

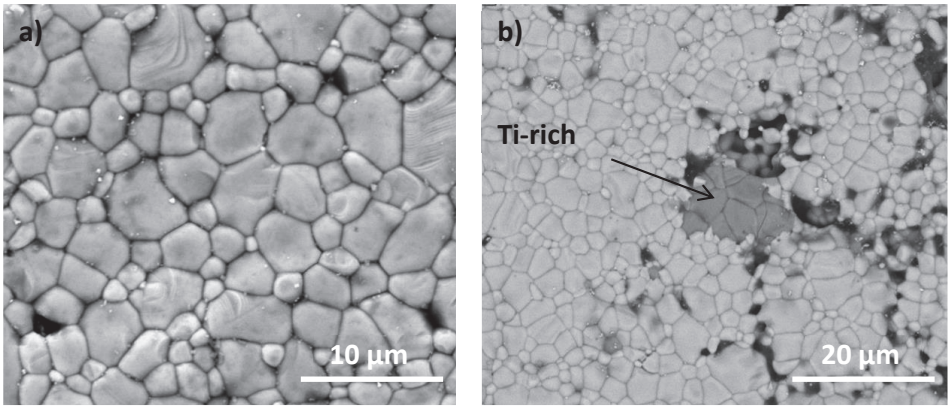

Figure 1: SEM images of the sintered $TiNb_2O_7$ tablets (a) and (b). Ti-rich spots (the central dark colour spot of picture (b)) were found from back scattered electron image in some regions of the sample surface.

The secondary phase was not observed by XRD due to its low concentration (Fig. 2). The measured patterns before and after the conductivity characterization match the reference pattern perfectly, showing that $TiNb_2O_7$ crystallizes in a rather complex monoclinic structure with space group A2/m and unit cell parameters: a=20.36 Å, b=3.80 Å, c=11.8861 Å, and β=120.19° as reported by Dreele and Cheetham [15]. Wadsley showed that each cation is coordinated by six oxygen ions in corner and/or edge sharing octahedrons, forming linear and zig-zag strings [16]. In general, Ti and Nb are randomly distributed and the cation sub-lattice is thus disordered.

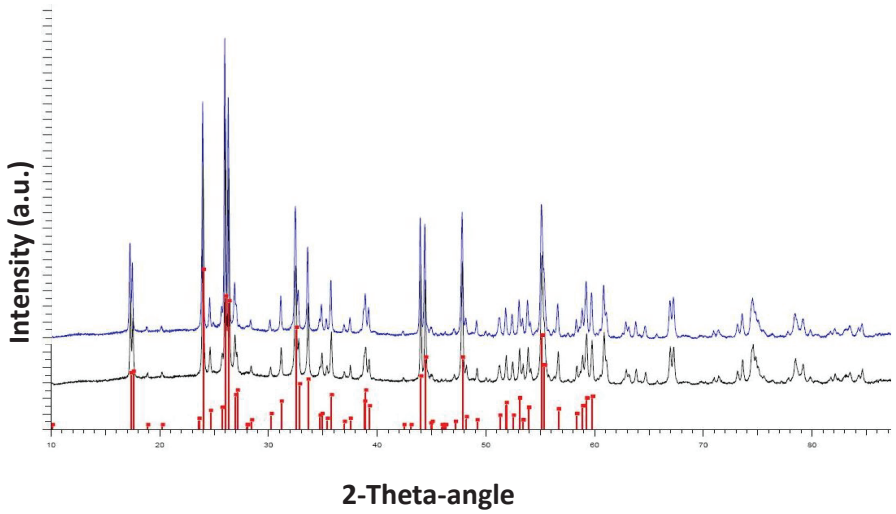

Figure 2: XRD patterns before (middle) and after (top) the conductivity measurement in oxygen atmospheres. The bottom patterns are the diffraction peaks of $TiNb_2O_7$ from the database of EVA program from 10^o to 60^o.

3.2 Electrical measurements

Fig. 3 presents the total conductivity in wet (~2.5% H_2O) and dry (~30 ppm H_2O) oxygen atmospheres in an Arrhenius representation, continuously recorded during cooling from 1100 to 450 °C at a rate of 12 °C/h. At temperatures above 750 ºC, there is no significant

difference in the conductivity between wet and dry conditions. However, below this temperature, the conductivity in wet atmosphere is slightly higher than that in dry atmosphere and the difference becomes more significant with decreasing temperature. This behavior would typically be interpreted as the contribution of protons to the total conductivity. However, as will be seen in the following discussion, this increase in conductivity is rather interpreted to reflect an increase in the electronic transport.

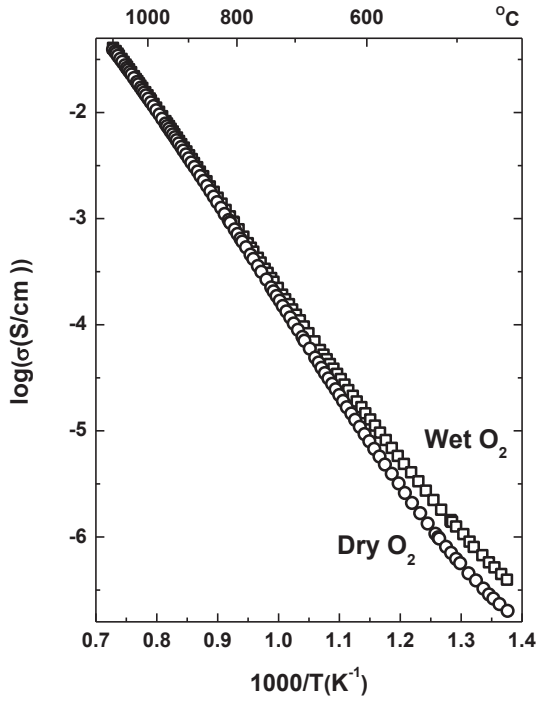

Figure 3: Temperature ramp of total conductivity in wet and dry oxidizing atmospheres from 1100 °C to 450 °C.

Fig. 4 shows the p_{O_2} dependencies of the total conductivity at different temperatures from 1000 °C to 600 °C under wet conditions (2.5% H_2O) in a log-log representation. The conductivity approaches a p_{O_2} independent region at low oxygen partial pressures and becomes essentially proportional to $p_{O_2}^{-1/4}$ at high oxygen partial pressures.

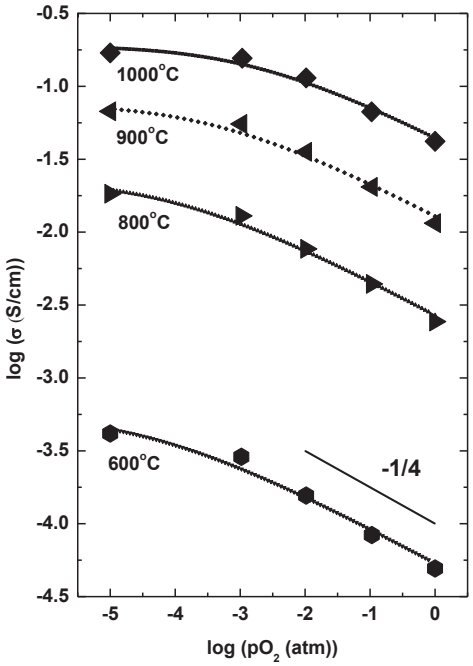

Figure 4: p_{O_2} dependencies of the total conductivity in wet conditions at various temperatures with fitted curves.

The total conductivity was also measured as a function of p_{H_2O} under oxidizing conditions (Fig. 5). The total conductivity increases gradually with increasing p_{H_2O} at low temperatures

whereas at temperatures above 700 ºC, the conductivity shows no significant change from dry to wet conditions - in agreement with the temperature ramps presented in Fig. 3.

The effect on the total conductivity by changing the atmosphere from O_2+2.5% D_2O to O_2+2.5% H_2O at 450 ºC is evident in Fig. 6. The ratio between the conductivities in these atmospheres is ~1.2 which indicates effects of protons on the conductivity.

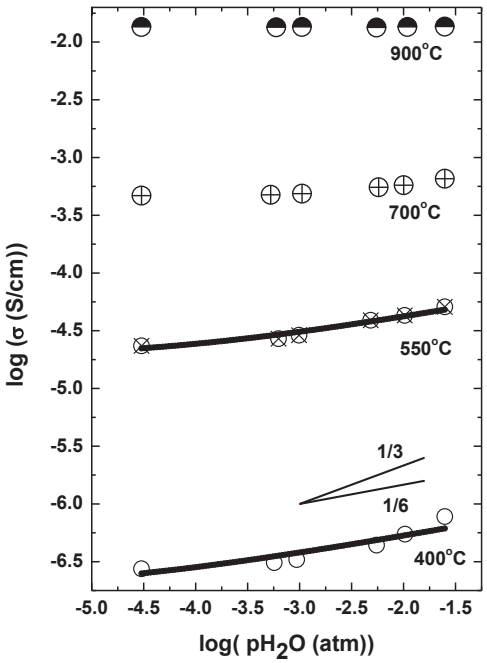

Figure 5: Total conductivity dependency on water vapor partial pressure at different temperatures. The fitted conductivity curves at low temperatures are shown as solid lines.

Proton transport numbers were calculated from the EMF induced by gradients in p_{O_2} and p_{H_2O} across the specimen. The maximum proton transport number was ~5%, (at 500 °C and

550 °C), considerably lower than expected from the isotope effect presented in Fig. 6. Isotope effects only qualitatively identify the contribution of proton conductivity, and taking the weak effect of water vapor on the conductivity (c.f. Fig. 5) into consideration, it is clear that the influence of proton conductivity in this material is not strong. Native ionic conductivity, such as oxygen ion transport was negligible. The total conductivity and divided partial proton conductivity based on the transport number measurements are shown in Fig. 7.

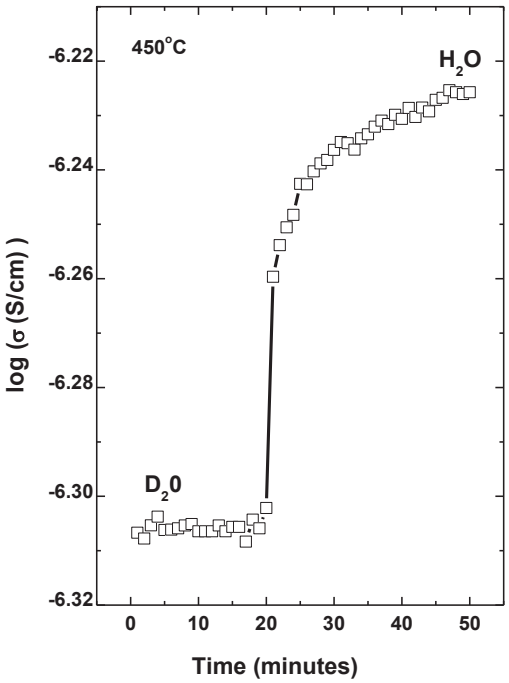

Figure 6: Effects on the conductivity of changes from D_2O to H_2O containing oxygen atmosphere.

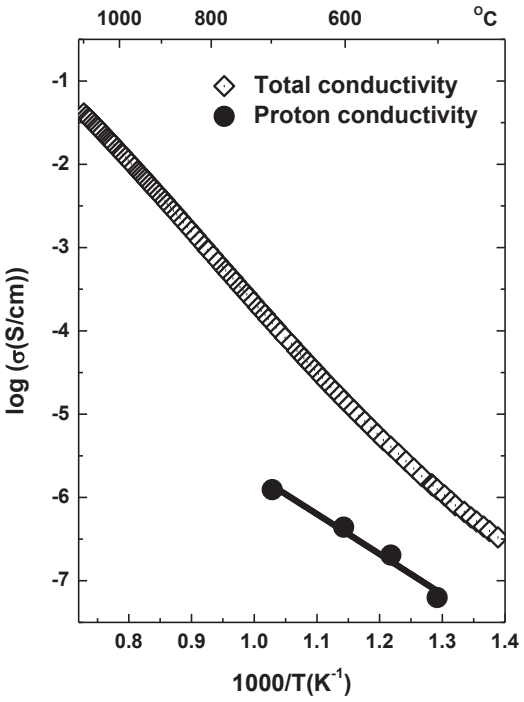

Figure 7: Total and partial proton conductivities as a function of the inverse absolute temperature in wet oxygen atmosphere. The solid line represents the fitted conductivity curve.

$TiNb_2O_7$ is known to be reduced to a rutile-type structured phase $TiNb_2O_6$, under reducing conditions giving rise to an increase in the total conductivity [17]. To investigate the transport properties of the sample in reducing atmospheres and the effects of this phase transition, the conductivity of the sample at 900 °C (cf. Fig.8) was recorded with a gradual change of p_{O_2}

by mixing argon with hydrogen under wet conditions. The conductivity is essentially independent of p_{O_2} between 10^{-5} and 10^{-11} atm followed by a small increase in conductivity going down to 10^{-13} atm. As p_{O_2} decreases further, the conductivity increases sharply by one order of magnitude reflecting the phase transition from $TiNb_2O_7$ to $TiNb_2O_6$. The conductivity of the reduced phase is essentially proportional to $p_{O_2}^{-1/6}$ indicating that native oxygen vacancies, charge compensated by electrons, constitute the majority defects.

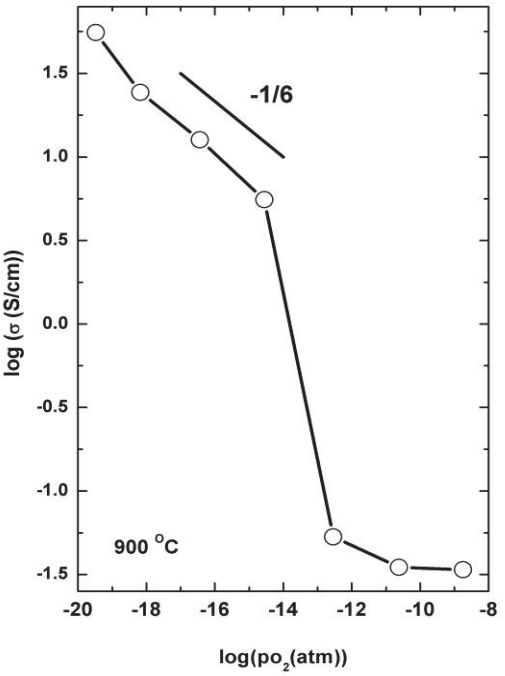

Figure 8: p_{O_2} dependency of total conductivity at 900 °C by four-point measurement in the phase transition region. The $p_{O_2}^{-1/6}$ relationship is found in low oxygen partial pressure region.

In order to identify the possibility of using the material as a hydrogen separation membrane, hydrogen flux measurements were attempted. However, the relatively large volume

difference between $TiNb_2O_7$ and $TiNb_2O_6$ at respectively the sweep and feed side, led to cracks along the edge of the sealing area which again resulted in a large leakage during the flux measurement.

4 Discussion

Based on the above observations, a defect chemical model for $TiNb_2O_7$ will now be proposed to which the conductivity data are fitted yielding thermodynamic and kinetic parameters describing the defect formation and migration.

4.1 Defect chemistry of the material

From the segregation of Ti-rich phases observed in SEM, it is concluded that the material is over-stoichiometric with respect to Nb. This results in donor doping and can be described in the Kröger-Vink notation as:

$$\frac{3}{2}Nb_2O_5 = Nb_{Ti}^{\bullet} + 2Nb_{Nb}^{x} + e^{/} + 7O_O^X + \frac{1}{4}O_2(g) \qquad (1)$$

Alternatively if the donors are assumed to be charge compensated by oxygen interstitials, donor doping can be written as:

$$3Nb_2O_5 = 2Nb_{Ti}^{\bullet} + 4Nb_{Nb}^{x} + 14O_O^X + O_i^{//} \qquad (2)$$

If we further assume that $v_O^{\bullet\bullet}$, $O_i^{//}$, $OH_O^{\bullet}$, $e^{/}$, $h^{\bullet}$, and $Nb_{Ti}^{\bullet}$ are the major possible point defects in $TiNb_2O_7$, the overall electroneutrality condition becomes

$$2[v_O^{\bullet\bullet}] + p + [OH_O^{\bullet}] + [Nb_{Ti}^{\bullet}] = n + 2[O_i^{//}] \qquad (3)$$

The defect reactions relating electrons and, respectively oxygen vacancies and oxygen interstitials, are

$$O_O^X = \frac{1}{2}O_2(g) + v_O^{\bullet\bullet} + 2e^{/} \qquad K_{vac} = [v_O^{\bullet\bullet}]n^2 p_{O_2}^{1/2} \tag{4}$$

and

$$\frac{1}{2}O_2(g) + 2e^{/} = O_i^{//} \qquad K_{int} = \frac{[O_i^{//}]}{n^2 p_{O_2}^{1/2}} \tag{5}$$

Generally, oxides are known to dissolve protons by hydration of oxygen vacancies:

$$H_2O(g) + v_O^{\bullet\bullet} + O_O^X = 2OH_O^{\bullet} \qquad K_{hv} = \frac{[OH_O^{\bullet}]^2}{[v_O^{\bullet\bullet}]p_{H_2O}} \tag{6}$$

In oxides that accommodate oxygen interstitials one may, however, foresee an alternative hydration mechanism where water is dissolved by interaction with lattice oxygen forming protons and oxygen interstitials as pairs that charge compensating each other:

$$H_2O(g) + 2O_O^X = 2OH_O^{\bullet} + O_i^{//} \quad K_{hi} = \frac{[O_i^{//}][OH_O^{\bullet}]^2}{P_{H_2O}} \tag{7}$$

For our $TiNb_2O_7$ specimen with Nb excess, the hydration reaction, Eq. (7), is likely to hold under the present experimental conditions, which is similar to the hydration mechanism reported for some related phosphates (TiP_2O_7, ZrP_2O_7, etc.) [8-10], and will be further discussed in the last part of this work.

By considering different limiting situations of the overall electroneutrality conditions (Eq. 3), the concentration dependencies of point defects on the oxygen and water vapor partial pressures can be derived by solving the equations above and illustrated graphically in so-called Brouwer diagrams shown in Figs. 9 and 10. Comparing the conductivity characteristics (cf. Figs. 4-5) and these diagrams, the experimental p_{O_2} -window seemingly corresponds to

the regime marked in Fig. 9, where the concentration of electrons changes from being independent of p_{O_2} to becoming proportional to $p_{O_2}^{-1/4}$. Although there are effects of water vapor and H/D isotope shifts on the conductivity, only small functional dependences being far from proportional to $p_{H_2O}^{1/3}$ (cf. Fig 10) were encountered, revealing that protons only have a weak influence on the total conductivity of the material. In the Brouwer diagram Fig. 10 the concentration dependency of minority electron is proportional to $p_{H_2O}^{1/6}$. Accordingly, the weak water vapor dependency could reflect increased electron conductivity. Proton conductivity may influence only at low temperatures and for the highest water vapor partial pressure applied.

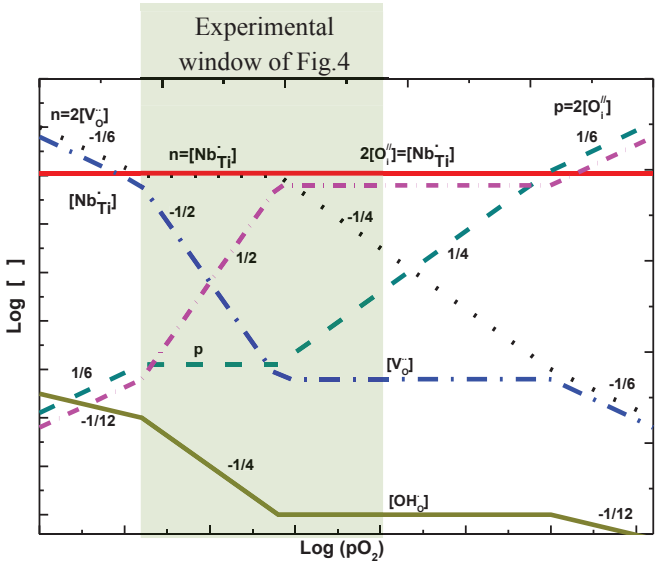

Figure 9: Brouwer diagram showing the oxygen partial pressure dependency of different defect concentrations in $TiNb_2O_7$. The slopes are calculated under the limiting electroneutralities indicated on the top part of the figure and the limiting electroneutrality window of our p_{O_2} measurement is included.

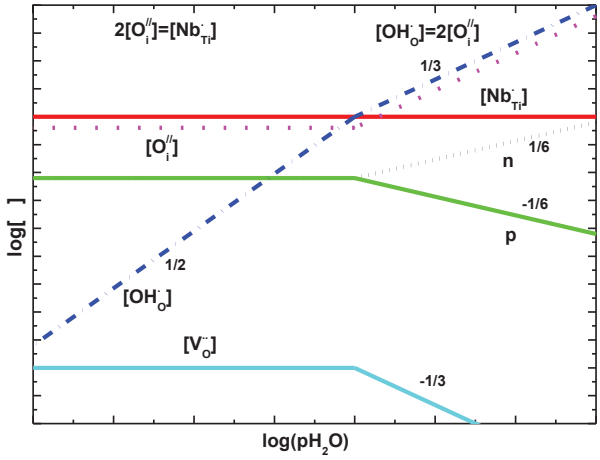

Figure 10: Brouwer diagram showing the water vapor dependency of different defect concentrations in $TiNb_2O_7$. The slopes are calculated under the limiting electroneutralities indicated on the top part of the figure.

4.2 Conductivity fitting

Generally, the conductivity of a charged species *i* can be expressed as

$$\sigma_i = z_i e c_i \mu_i \tag{8}$$

where z_i is the absolute charge of the species, e the elementary charge (C), c_i the concentration (cm^{-3}) and μ_i the mobility (cm^2/Vs). The mobility is, moreover, given by

$$\mu_i = \mu_{0,i} \frac{1}{T} \exp\left(\frac{-\Delta H_{mob,i}}{RT}\right) \tag{9}$$

where $\mu_{0,i}$ is the pre-exponential of charge mobility (cm^2K/Vs) and $\Delta H_{mob,i}$ the enthalpy of mobility.

To fit the p_{O_2} dependencies of the conductivity, expressions for the concentration of the predominating charge carriers are required. The electroneutrality of the majority defects within the measurement window at high temperatures is given by

$$2[O_i''] + n = [D^\bullet] \tag{10}$$

Protons are as such treated as minority defects in the high temperature regime. Combining Eq. 5 and Eq. 10 results in a quadratic equation from which the concentration of electrons is obtained as

$$n = \frac{-1 \pm \sqrt{1 - 8K_{int} p_{O_2}^{1/2}[D^\bullet]}}{4K_{int}\, p_{O_2}^{1/2}} \tag{11}$$

Under the assumption that electrons move as small polarons (Eq. 9), the electronic conductivity (n-type) can be expressed as:

$$\sigma_e = F \frac{-1 + \sqrt{1 - 8\exp\left(\frac{\Delta S_{int}}{R}\right)\exp\left(\frac{-\Delta H_{int}}{RT}\right) p_{O_2}^{1/2}[D^\bullet]}}{4\exp\left(\frac{\Delta S_{int}}{R}\right)\exp\left(\frac{-\Delta H_{int}}{RT}\right) p_{O_2}^{1/2}} \mu_e \tag{12}$$

where F is the Faraday constant. Moreover, since one half mole of gas is consumed in the reaction of Eq. 5, an entropy change of ~-60 J/mol K [18] was used as a first approximate input during the fitting of the total conductivity. By fitting this expression to the experimental data, values for ΔH_{int} and μ_e can be estimated. Furthermore, μ_e can be divided into a pre-exponential term $\mu_0(e)$ and the enthalpy of mobility for the electron $\Delta H_{mob}(e)$ by plotting μ_e at different temperatures in an Arrhenius representation.

In the case of fitting the p_{H_2O} dependencies of the conductivity in Fig. 5, it was assumed that protonic defects start to contribute concentration-wise at lower temperatures along with oxygen interstitials and donors yielding the electroneutrality

$$2[O_i''] = [OH_O^\bullet] + [D^\bullet] \tag{13}$$

Combining Eq. 7 and Eq. 13, a cubic equation is obtained:

$$4[O_i'']^3 - 4[D^\bullet][O_i'']^2 + [D^\bullet]^2[O_i''] - K_{hi}p_{H_2O} = 0 \tag{14}$$

Solving this equation, the concentration of oxygen interstitials can be expressed by the equilibrium constant of the hydration reaction in Eq. 7 and partial pressure of water:

$$[O_i''] = \frac{1}{6}\left(-[D^\bullet]^3 + 27K_{hi}p_{H_2O} + 3\sqrt{-6[D^\bullet]^3K_{hi}p_{H_2O} + 81K_{hi}^2p_{H_2O}^2}\right)^{1/3} + \frac{[D^\bullet]^2}{6\left(-[D^\bullet]^3 + 27K_{hi}p_{H_2O} + 3\sqrt{-6[D^\bullet]^3K_{hi}p_{H_2O} + 81K_{hi}^2p_{H_2O}^2}\right)^{1/3}} + \frac{1}{3}[D^\bullet] \tag{15}$$

The concentration of electrons can now be obtained by inserting Eq. 15 into Eq. 5. By using the extracted K_{int} and the parameters of electron mobility, the effects of p_{H_2O} on the total conductivity in Fig. 5 can be fitted to yield the contribution from partial electron conductivity from which, ΔH_{hi}, in the equation can be derived.

Finally, by using the values for ΔH_{int}, ΔH_{hi}, $\mu_0(e)$ and $\Delta H_{mob}(e)$ extracted above and listed in Table 1, a first approximation of the transport coefficients for the proton mobility can be estimated from fitting the partial proton conductivity in Fig. 7. The values are 11±10 cm^2/Vs for the pre-exponential and 74±8 kJ/mol for enthalpy of proton mobility.

Table 1: Summarized thermodynamic parameters of electron and proton defects in $TiNb_2O_7$

ΔS_{int} [J/mol K]	ΔH_{int} [kJ/mol]	$\mu_0(e)$ [cm^2/Vs]	$\Delta H_{mob}(e)$ [kJ/mol]	ΔS_{hi} [J/mol K]	ΔH_{hi} [kJ/mol]
-60±5	-134±5	$(3.4\pm1.1)\times10^5$	115±5	-120±5	-74±10

4.3 Hydration routes and material selecting

The exchange between water vapour and oxygen vacancies (Eq. 6) introduced by acceptor doping is by far the most reported reaction path in proton conducting oxides [2, 19-22], and only a limited number of materials have shown evidence to hydrate following the reaction in Eq. 7 [9, 10]. Stagnation in the search for new and good proton conductors among acceptor doped materials, however, calls for a better understanding of the materials properties related to the interstitial type of hydration. Consequently, we will discuss this mechanism in slightly more detail.

By taking anion disorder into account, the reaction in Eq. 7 is assumed to be active for two different classes of materials: i) oxides forming anti-Frenkel defects where hydration can be considered to occur as a combination of the conventional hydration reaction in Eq. 6 and the anti-Frenkel reaction, $O_O^X = O_i'' + v_O^{\bullet\bullet}$, and, ii) for oxides prone to form oxygen interstitials and where oxygen interstitials and protons could charge compensate each other with water vapor present.

In $TiNb_2O_7$, a relatively high anti-Frenkel formation energy was obtained from DFT calculations [23] indicating that formation of anti-Frenkel defects is rather unfavorable. Therefore, the second hydration mechanism, forming protons and oxygen interstitials together, could be the case. The thermodynamic values (cf. Table 1) estimated from fitting of

the conductivity data to this model indicate that $TiNb_2O_7$ can hold protons to relatively high temperatures. Although the uncertainty of the proton mobility data is high, it shows that proton migration is relatively activated and would therefore limit the proton conductivity.

The same type of hydration route as in $TiNb_2O_7$ and its influence on the electrical conductivity have been previously discussed in Y_2O_3 [24-26] with, however, electron hole conduction dominated situation under oxidizing atmospheres. At high water partial pressures, protons and oxygen interstitials are the majority defects charge compensated by each other. The electron hole conductivity shows a $p_{H_2O}^{-1/6}$ dependency. The proton conductivity was separated from the total conductivity by the same method (EMF method) as used in this work.

The concentration of protons in a material following the interstitial type of hydration will be highly dependent on the amount of interstitial positions that the structure could tolerate. Detailed structure analyses are needed to further clarify the amount of interstitial positions and to predict the maximum proton concentration. Although, few good proton conducting candidates with interstitial type of hydration have been found, the discussion still provides us an alternative view of searching for promising proton conducting oxides.

Conclusions

Over-stoichiometry of Nb in $TiNb_2O_7$ was observed giving self-donor-doping effect with respect to the material electrical properties. The conductivity of the $TiNb_2O_7$ is dominated by electronic conduction within the present experimental window. Under wet oxidizing condition, minor effects of proton conduction were confirmed by transport number measurement. An interstitial type of hydration reaction was suggested to explain the observed conductivity results and used for conductivity fitting. The enthalpy of hydration and the

parameters for electrons formation and migration were derived based on conductivity data – defect chemistry model fitting. A significant increase in conductivity was observed during the phase transition under reducing atmospheres from $TiNb_2O_7$ to $TiNb_2O_6$.

Acknowledgements

WX is grateful to the "BIGCO2" project of the Research Council of Norway (Climit 178004/I30, 176059/I30 and Gassnova 182070) with partners Statoil, GE Global Research, Statkraft, Aker Clean Carbon, Shell, TOTAL, ConocoPhillips, and ALSTOM. ZL acknowledges financial support from the Research Council of Norway under the project "Kinetics of High-Temperature Oxide Ion and Proton Conductors" (KINOXPRO) (RENERGI 190901/S60).

References

[1] H. Iwahara, T. Esaka, H. Uchida, N. Maeda, Proton conduction in sintered oxides and its application to steam electrolysis for hydrogen production, Solid State Ionics, 3–4 (1981) 359-363.
[2] R. Haugsrud, T. Norby, Proton conduction in rare-earth ortho-niobates and ortho-tantalates, Nat Mater, 5 (2006) 193-196.
[3] R. Haugsrud, Defects and transport properties in Ln_6WO_{12} (Ln=La, Nd, Gd, Er), Solid State Ionics, 178 (2007) 555-560.
[4] N. Kitamura, K. Amezawa, Y. Tomii, T. Hanada, N. Yamamoto, T. Omata, S. Otsuka-Yao-Matsuo, Electrical conduction properties of sr-doped $LaPO_4$ and $CePO_4$ under oxidizing and reducing conditions, Journal of the Electrochemical Society, 152 (2005) A658-A663.
[5] K. Amezawa, Y. Tomii, N. Yamamoto, High-temperature protonic conduction in $La_7P_3O_{18}$, Solid State Ionics, 175 (2004) 569-573.
[6] K. Amezawa, Y. Uchimoto, Y. Tomii, High temperature protonic conduction in Sr-doped LaP_3O_9, Solid State Ionics, 177 (2006) 2407-2411.
[7] T. Shimura, S. Fujimoto, H. Iwahara, Proton conduction in non-perovskite-type oxides at elevated temperatures, Solid State Ionics, 143 (2001) 117-123.
[8] V. Nalini, R. Haugsrud, T. Norby, High-temperature proton conductivity and defect structure of TiP_2O_7, Solid State Ionics, 181 (2010) 510-516.
[9] V. Nalini, M.H. Sørby, K. Amezawa, R. Haugsrud, H. Fjellvåg, T. Norby, Structure, water uptake, and electrical conductivity of TiP_2O_7, Journal of the American Ceramic Society, 94 (2011) 1514-1522.
[10] V. Nalini, K. Amezawa, W. Xing, T. Norby, High temperature proton conductivity of ZrP_2O_7, Journal of The Electrochemical Society, 157 (2010) B1491-B1498.
[11] T. Norby, Y. Larring, Mixed hydrogen ion–electronic conductors for hydrogen permeable membranes, Solid State Ionics, 136–137 (2000) 139-148.
[12] T. Norby, R. Haugsrud, Dense Ceramic Membranes for Hydrogen Separation, chapter 6, in: Membranes for Energy Conversion, Wiley-VCH Verlag GmbH & Co. KGaA, 2008, pp. 169-216.

[13] M. Amsif, A. Magrasó, D. Marrero-López, J.C. Ruiz-Morales, J. Canales-Vázquez, P. Núñez, Mo-Substituted lanthanum tungstate $La_{28-y}W_{4+y}O_{54+\delta}$: A competitive mixed electron–proton conductor for gas separation membrane applications, Chemistry of Materials, 24 (2012) 3868-3877.
[14] T. Norby, EMF method determination of conductivity contributions from protons and other foreign ions in oxides, Solid State Ionics, 28-30, Part 2 (1988) 1586-1591.
[15] R.B.V. Dreele, A.K. Cheetham, The Structures of Some Titanium-Niobium Oxides by Powder Neutron Diffraction, Proceedings of the Royal Society of London. A. Mathematical and Physical Sciences, 338 (1974) 311-326.
[16] A. Wadsley, Mixed oxides of titanium and niobium. I, Acta Crystallographica, 14 (1961) 660-664.
[17] C.M. Reich, A. Kaiser, J.T.S. Irvine, Niobia Based Rutile Materials as SOFC Anodes, Fuel Cells, 1 (2001) 249-255.
[18] T. Norby, M. Widerøe, R. Glöckner, Y. Larring, Hydrogen in oxides, Dalton Transactions, (2004) 3012-3018.
[19] K.H. Ryu, S.M. Haile, Chemical stability and proton conductivity of doped $BaCeO_3$–$BaZrO_3$ solid solutions, Solid State Ionics, 125 (1999) 355-367.
[20] G.C. Mather, M.S. Islam, Defect and Dopant Properties of the $SrCeO_3$-Based Proton Conductor, Chemistry of Materials, 17 (2005) 1736-1744.
[21] R. Haugsrud, T. Norby, High-temperature proton conductivity in acceptor-doped $LaNbO_4$, Solid State Ionics, 177 (2006) 1129-1135.
[22] S.-J. Song, H.-S. Park, Mixed pronton–electron conducting properties of Yb doped strontium cerate, Journal of Materials Science, 42 (2007) 6177-6182.
[23] L.-E. Kalland, Master Thesis, University of Oslo, (2010).
[24] T. Norby, P. Kofstad, Proton and native-ion conductivities in Y_2O_3 at high temperatures, Solid State Ionics, 20 (1986) 169-184.
[25] T. Norby, P.E.R. Kofstad, Electrical Conductivity and Defect Structure of Y_2O_3 as a Function of Water Vapor Pressure, Journal of the American Ceramic Society, 67 (1984) 786-792.
[26] T. Norby, P.E.R. Kofstad, Direct-Current conductivity of Y_2O_3 as a function of water vapor pressure, Journal of the American Ceramic Society, 69 (1986) 780-783.

Manuscript V

Electrical characterization of compounds with different structures in La_2O_3-TiO_2 phase diagram

Wen Xing

V

References for Summery, Chapters1-4 and 6

[1] V. Nalini, M.H. Sørby, K. Amezawa, R. Haugsrud, H. Fjellvåg, T. Norby, Structure, water uptake, and electrical conductivity of TiP_2O_7, Journal of the American Ceramic Society, 94 (2011) 1514-1522.
[2] V. Nalini, K. Amezawa, W. Xing, T. Norby, High temperature proton conductivity of ZrP_2O_7, Journal of The Electrochemical Society, 157 (2010) B1491-B1498.
[3] R. Haugsrud, T. Norby, Mixed ionic-electronic conductivity in Ca doped $La_2Ti_2O_7$, Proc. Risø International Conf. on Solid State Electrochemistry, (2005) 209.
[4] R. Haugsrud, Defects and transport properties in Ln_6WO_{12} (Ln=;La, Nd, Gd, Er), Solid State Ionics, 178 (2007) 555-560.
[5] R. Haugsrud, C. Kjølseth, Effects of protons and acceptor substitution on the electrical conductivity of La_6WO_{12}, Journal of Physics and Chemistry of Solids, 69 (2008) 1758-1765.
[6] R. Haugsrud, T. Norby, High-temperature proton conductivity in acceptor-doped $LaNbO_4$, Solid State Ionics, 177 (2006) 1129-1135.
[7] R. Haugsrud, T. Norby, Proton conduction in rare-earth ortho-niobates and ortho-tantalates, Nat Mater, 5 (2006) 193-196.
[8] G.C. Mather, M.S. Islam, Defect and Dopant Properties of the $SrCeO_3$-Based Proton Conductor, Chemistry of Materials, 17 (2005) 1736-1744.
[9] K.H. Ryu, S.M. Haile, Chemical stability and proton conductivity of doped $BaCeO_3$–$BaZrO_3$ solid solutions, Solid State Ionics, 125 (1999) 355-367.
[10] H. Iwahara, T. Esaka, H. Uchida, N. Maeda, Proton conduction in sintered oxides and its application to steam electrolysis for hydrogen production, Solid State Ionics, 3–4 (1981) 359-363.
[11] H. Iwahara, Oxide-ionic and protonic conductors based on perovskite-type oxides and their possible applications, Solid State Ionics, 52 (1992) 99-104.
[12] G. Ma, T. Shimura, H. Iwahara, Ionic conduction and nonstoichiometry in $BaCe_{0.90}Y_{0.10}O_{3-\alpha}$, Solid State Ionics, 110 (1998) 103-110.
[13] N. Taniguchi, K. Hatoh, J. Niikura, T. Gamo, H. Iwahara, Proton conductive properties of gadolinium-doped barium cerates at high temperatures, Solid State Ionics, 53–56, Part 2 (1992) 998-1003.
[14] T. Yajima, H. Kazeoka, T. Yogo, H. Iwahara, Proton conduction in sintered oxides based on $CaZrO_3$, Solid State Ionics, 47 (1991) 271-275.
[15] J.W. Phair, S.P.S. Badwal, Materials for separation membranes in hydrogen and oxygen production and future power generation, Sci Technol Adv Mat, 7 (2006) 792-805.
[16] T. Norby, R. Haugsrud, Dense Ceramic Membranes for Hydrogen Separation, chapter 6, in: Membranes for Energy Conversion, Wiley-VCH Verlag GmbH & Co. KGaA, 2008, pp. 169-216.
[17] J.C. Boivin, G. Mairesse, Recent Material Developments in Fast Oxide Ion Conductors, Chemistry of Materials, 10 (1998) 2870-2888.
[18] T.H. Etsell, S.N. Flengas, Electrical properties of solid oxide electrolytes, Chemical Reviews, 70 (1970) 339-376.
[19] J.W. Stevenson, K. Hasinska, N.L. Canfield, T.R. Armstrong, Influence of cobalt and iron additions on the electrical and thermal properties of $(La,Sr)(Ga,Mg)O_{3-\delta}$, Journal of The Electrochemical Society, 147 (2000) 3213-3218.
[20] J.W. Fergus, Electrolytes for solid oxide fuel cells, Journal of Power Sources, 162 (2006) 30-40.
[21] J.B. Goodenough, Oxide-ion electrolytes, Annual Review of Materials Research, 33 (2003) 91-128.
[22] S. Stotz, C. Wagner, Die Löslichkeit von Wasserdampf und Wasserstoff in festen Oxiden, Berichte der Bunsengesellschaft für physikalische Chemie, 70 (1966) 781-788.
[23] K.D. Kreuer, Pronton-conducting oxides, Annual Review of Materials Research, 33 (2003) 333-359.

[24] T. Hibino, K. Mizutani, T. Yajima, H. Iwahara, Characterization of proton in Y-doped $SrZrO_3$ polycrystal by IR spectroscopy, Solid State Ionics, 58 (1992) 85-88.
[25] H.G. Bohn, T. Schober, T. Mono, W. Schilling, The high temperature proton conductor $Ba_3Ca_{1.18}Nb_{1.82}O_{9-\delta}$. I. Electrical conductivity, Solid State Ionics, 117 (1999) 219-228.
[26] E. Quarez, S. Noirault, M.T. Caldes, O. Joubert, Water incorporation and proton conductivity in titanium substituted barium indate, Journal of Power Sources, 195 (2010) 1136-1141.
[27] T. Norby, P. Kofstad, Proton and native-ion conductivities in Y_2O_3 at high temperatures, Solid State Ionics, 20 (1986) 169-184.
[28] T. Norby, O. Dyrlie, P. Kofstad, Protonic conduction in acceptor-doped cubic rare-earth sesquioxides, Journal of the American Ceramic Society, 75 (1992) 1176-1181.
[29] T. Norby, O. Dyrlie, P. Kofstad, Protons in Ca-doped La_2O_3, Nd_2O_3 and $LaNdO_3$, Solid State Ionics, 53–56, Part 1 (1992) 446-452.
[30] T. Omata, S. Otsuka-Yao-Matsuo, Electrical properties of proton-conducting Ca^{2+} -doped $La_2Zr_2O_7$ with a pyrochlore-type structure, Journal of The Electrochemical Society, 148 (2001) E252-E261.
[31] R. Hancke, A. Magrasó, T. Norby, R. Haugsrud, Hydration of lanthanum tungstate (La/W = 5.6 and 5.3) studied by TG and simultaneous TG-DSC, Solid State Ionics, Submitted manuscript (2012).
[32] A. Magraso, J.M. Polfus, C. Frontera, J. Canales-Vazquez, L.-E. Kalland, C.H. Hervoches, S. Erdal, R. Hancke, M.S. Islam, T. Norby, R. Haugsrud, Complete structural model for lanthanum tungstate: a chemically stable high temperature proton conductor by means of intrinsic defects, Journal of Materials Chemistry, 22 (2012) 1762-1764.
[33] N. Sharova, H. Fjellvåg, T. Norby, Structure, defect chemistry, and proton conductivity in nominally Sr-doped $Ba_3La(PO_4)_3$, Solid State Ionics, 180 (2009) 338-342.
[34] R. Gerhardt-Anderson, A.S. Nowick, Ionic conductivity of CeO_2 with trivalent dopants of different ionic radii, Solid State Ionics, 5 (1981) 547-550.
[35] P.S. Manning, J.D. Sirman, R.A. De Souza, J.A. Kilner, The kinetics of oxygen transport in 9.5 mol % single crystal yttria stabilised zirconia, Solid State Ionics, 100 (1997) 1-10.
[36] M. Huse, T. Norby, R. Haugsrud, Effects of A and B site acceptor doping on hydration and proton mobility of $LaNbO_4$, International Journal of Hydrogen Energy, 37 (2012) 8004-8016.
[37] F.W. Poulsen, Speculations on the existence of hydride ions in proton conducting oxides, Solid State Ionics, 145 (2001) 387-397.
[38] H.U. Anderson, Review of p-type doped perovskite materials for SOFC and other applications, Solid State Ionics, 52 (1992) 33-41.
[39] T. Norby, M. Widerøe, R. Glöckner, Y. Larring, Hydrogen in oxides, Dalton Transactions, (2004) 3012-3018.
[40] T. Norby, A Kröger-Vink compatible notation for defects in inherently defective sublattices, Journal of the Korean Ceramic Society, 47 (2010) 19-25.
[41] S. Erdal, L.-E. Kalland, R. Hancke, J. Polfus, R. Haugsrud, T. Norby, A. Magrasó, Defect structure and its nomenclature for mixed conducting lanthanum tungstates $La_{28-x}W_{4+x}O_{54+3x/2}$, International Journal of Hydrogen Energy, 37 (2012) 8051-8055.
[42] R. Strandbakke, C. Kongshaug, R. Haugsrud, T. Norby, High-temperature hydration and conductivity of mayenite, $Ca_{12}Al_{14}O_{33}$, The Journal of Physical Chemistry C, 113 (2009) 8938-8944.
[43] S.J. Song, E.D. Wachsman, J. Rhodes, H.S. Yoon, K.H. Lee, G. Zhang, S.E. Dorris, U. Balachandran, Hydrogen permeability and effect of microstructure on mixed protonic-electronic conducting Eu-doped strontium cerate, Journal of Materials Science, 40 (2005) 4061-4066.
[44] X. Qi, Y.S. Lin, Electrical conduction and hydrogen permeation through mixed proton–electron conducting strontium cerate membranes, Solid State Ionics, 130 (2000) 149-156.
[45] U. Balachandran, T.H. Lee, S.E. Dorris, Hydrogen production by water dissociation using mixed conducting dense ceramic membranes, International Journal of Hydrogen Energy, 32 (2007) 451-456.
[46] A.V. Virkar, Transport of H_2, O_2 and H_2O through single-phase, two-phase and multi-phase mixed proton, oxygen ion, and electron hole conductors, Solid State Ionics, 140 (2001) 275-283.

[47] S. Hamakawa, L. Li, A. Li, E. Iglesia, Synthesis and hydrogen permeation properties of membranes based on dense $SrCe_{0.95}Yb_{0.05}O_{3-\alpha}$ thin films, Solid State Ionics, 148 (2002) 71-81.
[48] T. Norby, EMF method determination of conductivity contributions from protons and other foreign ions in oxides, Solid State Ionics, 28-30, Part 2 (1988) 1586-1591.
[49] F.T. Miles, A.W.C. Menzies, The Vapor Pressure of Deuterium Water from 20 to 230°, Journal of the American Chemical Society, 58 (1936) 1067-1069.
[50] Sossina M. Haile, D.L. West, J. Campbel, The role of microstructure and processing on the proton conducting properties of gadolinium-doped barium cerate, Journal of Materials Research, 13 (1998) 1576-1595.
[51] B.A. Boukamp, Equivalent circuit for Windows Ver.1.2, 2008.
[52] V. Nalini, Ph.D thesis, University of Oslo, (2010).
[53] K.D. Kreuer, S. Adams, W. Münch, A. Fuchs, U. Klock, J. Maier, Proton conducting alkaline earth zirconates and titanates for high drain electrochemical applications, Solid State Ionics, 145 (2001) 295-306.
[54] K.D. Kreuer, Aspects of the formation and mobility of protonic charge carriers and the stability of perovskite-type oxides, Solid State Ionics, 125 (1999) 285-302.
[55] S. Erdal, Ph.D Thesis, University of oslo, (2011).
[56] L. Leon-Reina, J.M. Porras-Vazquez, E.R. Losilla, D.V. Sheptyakov, A. Llobet, M.A.G. Aranda, Low temperature crystal structures of apatite oxygen-conductors containing interstitial oxygen, Dalton Transactions, (2007) 2058-2064.
[57] M. Yashima, H. Yamada, S. Nuansaeng, T. Ishihara, Role of Ga^{3+} and Cu^{2+} in the high interstitial oxide-ion diffusivity of Pr_2NiO_4-based oxides: design concept of interstitial ion conductors through the higher-valence d10 dopant and Jahn–Teller effect, Chemistry of Materials, 24 (2012) 4100-4113.
[58] W. Paulus, A. Cousson, G. Dhalenne, J. Berthon, A. Revcolevschi, S. Hosoya, W. Treutmann, G. Heger, R. Le Toquin, Neutron diffraction studies of stoichiometric and oxygen intercalated La_2NiO_4 single crystals, Solid State Sciences, 4 (2002) 565-573.
[59] A. Demourgues, A. Wattiaux, J.C. Grenier, M. Pouchard, J.L. Soubeyroux, J.M. Dance, P. Hagenmuller, Electrochemical preparation and structural characterization of $La_2NiO_{4+\delta}$ phases ($0 \leqslant \delta \leqslant 0.25$), Journal of Solid State Chemistry, 105 (1993) 458-468.
[60] A. Grimaud, F. Mauvy, J. Marc Bassat, S. Fourcade, M. Marrony, J. Claude Grenier, Hydration and transport properties of the $Pr_{2-x}Sr_xNiO_{4+\delta}$ compounds as H^+-SOFC cathodes, Journal of Materials Chemistry, 22 (2012) 16017-16025.
[61] T. Norby, P.E.R. Kofstad, Electrical Conductivity and Defect Structure of Y_2O_3 as a Function of Water Vapor Pressure, Journal of the American Ceramic Society, 67 (1984) 786-792.
[62] T. Norby, P.E.R. Kofstad, Direct-Current conductivity of Y_2O_3 as a function of water vapor pressure, Journal of the American Ceramic Society, 69 (1986) 780-783.
[63] T. Norby, Fast oxygen ion conductors-from doped to ordered systems, Journal of Materials Chemistry, 11 (2001) 11-18.
[64] V. Besikiotis, C.S. Knee, I. Ahmed, R. Haugsrud, T. Norby, Crystal structure, hydration and ionic conductivity of the inherently oxygen-deficient $La_2Ce_2O_7$, Solid State Ionics, 228 (2012) 1-7.
[65] R. Haugsrud, H. Fjeld, K.R. Haug, T. Norby, Mixed Ionic and Electronic Conductivity of Undoped and Acceptor-Doped Er_6WO_{12}, Journal of The Electrochemical Society, 154 (2007) B77-B81.
[66] J. Nell, B. J. Wood, High-temperature electrical measurements and thermodynamic properties of Fe_3O_4-$FeCr_2O_4$-$MgCr_2O_4$-$FeAl_2O_4$ spinels, American Mineralogist, 76 (1991) 405-426.
[67] L. Minervini, R.W. Grimes, K.E. Sickafus, Disorder in Pyrochlore Oxides, Journal of the American Ceramic Society, 83 (2000) 1873-1878.